

Asymptotic theory for the dynamic of networks with heterogenous social capital allocation

Enrico Ubaldi^{1,2}, Nicola Perra^{3,4}, Márton Karsai⁵, Alessandro Vezzani^{1,6}, Raffaella Burioni^{1,2}, and Alessandro Vespignani⁴

¹*Dipartimento di Fisica e Scienza della Terra, Università di Parma, Parco Area delle Scienze 7/A, 43124 Parma, Italy*

²*INFN, Gruppo Collegato di Parma, Parco Area delle Scienze 7/A, 43124 Parma, Italy*

³*Centre for Business Network Analysis, University of Greenwich, Park Row, London SE10 9LS, United Kingdom*

⁴*Laboratory for the Modeling of Biological and Socio-technical Systems, Northeastern University, Boston MA 02115 USA*

⁵*Laboratoire de l'Informatique du Parallélisme, INRIA-UMR 5668, IXXI, ENS de Lyon, 69364 Lyon, France*

⁶*Centro S3, CNR-Istituto di Nanoscienze, Via Campi 213A, 41125 Modena Italy*

Abstract

The structure and dynamic of social network are largely determined by the heterogeneous interaction activity and social capital allocation of individuals. These features interplay in a non-trivial way in the formation of network and challenge a rigorous dynamical system theory of network evolution. Here we study seven real networks describing temporal human interactions in three different settings: scientific collaborations, Twitter mentions, and mobile phone calls. We find that the node's activity and social capital allocation can be described by two general functional forms that can be used to define a simple stochastic model for social network dynamic. This model allows the explicit asymptotic solution of the Master Equation describing the system dynamic, and provides the scaling laws characterizing the time evolution of the social network degree distribution and individual node's ego network. The analytical predictions reproduce with accuracy the empirical observations validating the theoretical approach. Our results provide a rigorous dynamical system framework that can be extended to include other features of networks' formation and to generate data driven predictions for the asymptotic behavior of large-scale social networks.

The formation of social networks requires invest-

ments in time and energy by each individual actor with the anticipation that collective benefits can arise for individuals and groups. Individuals however invest in developing social interactions heterogeneously and according to very diverse strategies. In the first place not all individuals are equally active in a given social network. Furthermore, individuals may allocate their social capital in very diverse way, for instance by favoring the strengthening of a limited number of strong ties (bonding capital) as opposed to favor the exploration of weak ties opening access to new information and communities (bridging capital) [1, 2, 3, 4, 5, 6, 7, 8]. The origins of such heterogeneities are rooted in the trade off between competing factors such as the need for close relationships [9], the efforts required to keep social ties [10], temporal and cognitive constraints [11, 12, 13], and have long been acknowledged as key elements in the description of social networks' properties [14, 15, 16], dynamical features [17, 18, 19, 20, 21, 22, 23, 24, 15, 25], and the behavior of processes unfolding in social systems [14, 15, 16, 17, 26, 27, 28, 29, 30, 31, 32]. However, it is still lacking a general dynamical system framework able to relate the emerging connectivity pattern of social networks to the combined action of

social actors activity and their heterogeneity in distributing resources in social capital allocation.

Here we analyze seven time-resolved datasets describing three different types of social interactions: scientific collaborations, Twitter mentions, and mobile phone calls. For all network datasets we define two functions statistically encoding the instantaneous activity of nodes and the allocation of social capital, respectively. The latter function is regulated by two parameters - system dependent- that define a simple reinforcement mechanism. In particular we observe in all datasets that the larger the number of social ties already activated by each node and the smaller is the probability of creating a new tie. We provide a thorough statistical characterization of the activity and reinforcement dynamics at play in each network and identify the basic parameters defining the dynamic of ties evolution.

Prompted by this statistical analysis, we propose a dynamic network model that includes the heterogeneous activity of nodes and the tie formation mechanisms. This model allows the definition of a formal Master Equation (ME) describing the evolution of the network connectivity structure that can be solved in the asymptotic regime (large network size and long time evolution). The solution of the ME provides the asymptotic form the degree distribution and the scaling relations relating degree, activity and the functions characterizing the social capital allocation. The analytical solutions are capturing very well the empirical behavior measured in the analyzed datasets, connecting explicitly the evolution of social networks to the parameter regulating the emergence of heterogeneous social ties. The proposed analytical framework is remarkably general and it can be solved for statistically different activity patterns. The presented results have the potential to open the path to a general asymptotic theory of the dynamic of social networks by progressively integrating further social capital allocation strategies for the formation of social ties.

1 Results

We analyze seven datasets containing time-stamped information about three different type of social interactions: scientific collaborations, Twitter mentions, and mobile phone calls. While we refer the reader to the Material and Methods section for the details of each data set, we represent all datasets as time-varying networks. Each node describes an individual. Each time-resolved link describes a social act. The nature of connections is different according to the specific dataset. Links might represent a collaboration resulting in a publication in a scientific journal, a Twitter mention, or a mobile phone call. We considered five scientific collaborations networks obtained from five different journals (*PRA*, *PRB*, *PRD*, *PRE*, and *PRL*) of the American Physical Society (APS), one Twitter mentions network (*TMN*), and one mobile phone network (*MPN*).

In order to characterize the time-varying properties of such networks we first measure the activity a_i . Formally, a_i is defined as the fraction of interactions in which node i is engaged per unit of time with respect to all the interactions per unit time occurring in the network. This quantity describes the propensity of nodes i to be involved in social interactions. Empirical measurements in a wide set of social networks show broad distributions of activity [23, 28, 29, 16, 33]. As shown in Figure 1 [A-D], we confirm these observations in our datasets. In particular we find that in the APS and MPN datasets the activity is well fitted by a truncated power law, while in the TMN we find a Log-Normal distribution (see Material and Methods and Supplementary Online Materials for details).

1.1 Social capital allocation

The activity a_i sets the clock for the activation of each node, however it does not provide any information on how each node invests its social capital in exploring new ties or reinforcing already established ties [34]. In order to measure the formation of new ties, we group nodes in classes with similar activity a and final degree k , so that each class b contains actors with statistically equivalent characteristics (see

SI for details). We then measure the probability $p_b(k)$ that the next social act for the nodes in the class b that have already contacted k nodes will result in the establishment of a new, $k + 1$ -th, tie. As shown in Figure 1 [E-H] $p_b(k)$ is in general a decreasing function of k . This observation resonates with previous research and empirical findings suggesting that our social interactions are bounded by cognitive and temporal constraints [10, 11, 12, 13]. Indeed, the larger the number of alters in our social circle, the smaller the probability that the next social act will be towards a new tie.

The above empirical findings suggest that the mechanism governing the allocation of social capital follow a general form that in its simplest analytical form can be written as:

$$p_b(k) = \left(1 + \frac{k}{c_b}\right)^{-\beta_b}. \quad (1)$$

In this expression, β_b modulate the tendency to explore new connections, while c_b define the intrinsic characteristic limit of the individual to maintain multiple ties. Although one could imagine more complicate analytical forms, we use this parsimonious approach to characterize the different data sets. Interestingly, we find that in the five co-authorship networks and Twitter, the exponent β is the same regardless of the class b . Furthermore, the values of c_b are typically peaked around a well defined value (see SI for details). More in detail, we can rescale the proposed functional form in each class b by defining the variable $x_b = k/c_b$, yielding

$$p_b(x_b)^{\frac{1}{\beta}} = (1 + x_b)^{-1}. \quad (2)$$

In the presence of a single exponent β characterizing the system, as shown in Figure 1 [I-K], all empirical curves do collapse on the reference function $(1+x)^{-1}$. The data collapse however is not occurring in the case of the MPN dataset. In the latter we find a more heterogeneous scenario in which different nodes' classes are characterized by different values of β_b and c_b , see Figure 1 L. In the Supplementary Online Material we provide further evidence for the evidence of a single or distributed value of β in different datasets.

1.2 Stochastic model for the network dynamic

By leveraging on the empirical evidence gathered here, it is possible to define a basic generative model of network formation based on two stochastic processes. Defined the network \mathcal{G} containing N nodes, at each time step a node i is active according to a probability a_i drawn from distribution $F(a)$. [23, 28, 29, 16, 33]. Once active, the node i that has already contacted k different agents will contact a new, randomly chosen node with probability $p_i(k) = (1 + k/c_i)^{-\beta_i}$. Otherwise, with probability $1 - p_i(k)$, it will interact with an already contacted node chosen at random. Interactions are considered to last one single time step. For this model it is possible to write explicitly the master equation (ME) describing the evolution of the probability distribution $P_i(k, t)$ that a node i has degree k at time t :

$$\begin{aligned} P_i(k, t+1) = & P_i(k-1, t) \left[a_i p_i(k-1) + \sum_{j \sim i} a_j \sum_{k_j} \frac{p_j(k_j)}{(N-j)} P_j(k_j, t) \right] + \\ & P_i(k, t) \left[a_i [1 - p_i(k)] + \sum_{j \sim i} a_j \sum_{k_j} \left(1 - \frac{p_j(k_j)}{(N-j)} \right) P_j(k_j, t) \right] + \\ & P_i(k, t) \left[1 - \sum_j a_j \right]. \end{aligned} \quad (3)$$

In the above equation $j \sim i$ and $j \approx i$ are the sum over the nodes already contacted and not yet contacted by i , respectively. Within these sums, we use k_j as the degree of the node j . The first two terms on the right hand side of Eq. (3) account for the creation of nodes of degree k which occurs when a node of degree $k-1$ gets active and contacts a new node, or when it gets in contact with a new node of previous degree k_j that activates and attaches to node i . The third and fourth terms of the r.h.s. of the equation account for the conservation of nodes of degree k , i.e. nodes that either get active and contact one of their neighbors with probability $a(1-p(k))$ or get contacted by one of their neighbors. The last line of Eq. (3) takes into account for the case in which no node gets active in the current evolution time step, thus conserving the $P_i(k, t)$.

1.3 Asymptotic theory for network with $\beta_b = \beta$

In the case of networks characterized by a single exponent β it is possible to consider for the ME the large time and large k limit, so that k can be approximated by a continuous variable. By neglecting the subleading terms of order $1/t$ we can thus write the continuous asymptotic version of Eq. (3) as

$$\frac{\partial P}{\partial t} = -\frac{ac^\beta}{k^\beta} \frac{\partial P}{\partial k} + \frac{ac^\beta}{2k^\beta} \frac{\partial^2 P}{\partial k^2} + \frac{a\beta c^\beta}{k^{\beta+1}} P(a, k, t) + \left(\frac{1}{2} \frac{\partial^2 P}{\partial k^2} - \frac{\partial P}{\partial k} \right) \int da \rho(a) a \int dh \frac{c^\beta}{h^\beta} P(a, h, t). \quad (4)$$

This equation can be solved explicitly (see SI for details), yielding the asymptotic form:

$$P_i(k, t) = A \exp \left[-\frac{\left(k - B(a_i, c_i) t^{\frac{1}{1+\beta}} \right)^2}{C t^{\frac{1}{1+\beta}}} \right], \quad (5)$$

where A is a normalization constant, C a constant and $B(a_i, c_i)$ a multiplicative factor of the $t^{1/(1+\beta)}$ term that depends on the activity a_i and c_i of the considered agent. Its implicit expression is given in the SI.

A first general result concerns the evolution in time of the average degree $\langle k(a, t) \rangle$ of nodes belonging to a given activity class that follows the scaling laws

$$\langle k(a, t) \rangle \propto (at)^{\frac{1}{1+\beta}}. \quad (6)$$

The growth of the system is thus modulated by the parameter β that sets the strength of the reinforcement process in the process ruling the establishment of new social ties. In the limit case $\beta = 0$ the growth would be linear. Indeed, the reinforcement of previously activated ties would be zero and nodes would keep connecting randomly to other vertices, thus increasing indefinitely their social circle. In the opposite limit $\beta \rightarrow \infty$ each node would invest its social capital on just one single connection, i.e. the first established. In the six datasets described by a single β value, we observe the range $0.13 \leq \beta \leq 0.47$ that indicates a sub-linear growth of the social system. In Figure S12 we find a very good agreement between the analytical prediction of Eq. (6) and the

empirical $\langle k(a, t) \rangle$ curves, obtaining the first empirical validation of the modeling framework proposed and its ability at capturing the network formation dynamic.

Furthermore, Eq. (6) connects, at a given time t , the degree k and the activity a of a given node, as $k \propto a^{\frac{1}{1+\beta}}$. Thus, given any specific activity distribution $F(a)$, we can infer the functional form of the degree distribution $\rho(k)$ by substituting $a \rightarrow k^{\frac{1}{1+\beta}}$, finding:

$$\rho(k) dk \propto F(k^{(1+\beta)}) k^\beta dk. \quad (7)$$

It is important stressing that the analytical framework is not limited to a specific functional form of the activity. Indeed, with an arbitrary functional form of $F(a)$, Eq. (6) gives us the possibility to predict the behavior and parameters of the corresponding degree distribution. In Table 3 we report the degree distribution predicted by Eq. (6) for activities following a common set of heavy-tailed distributions, i.e. power-laws, truncated power-law, stretched exponentials, and log-normal, that are usually found in empirical data. In Figure S12[E-G] we compare the degree distributions $\rho(k)$ predicted by Eq. (S22) with real data. Interestingly, also in this case the functional form obtained from the analytical solution of the model fit remarkably well the empirical evidence. It is important to notice that $\rho(k)$ is also function of the parameter β . In other words, the connectivity patterns emerging from social interactions can be inferred knowing the propensity of individuals to be involved in social acts, the activity, and the strength of the reinforcement towards previously established ties, β . Finally it is worth remarking that Eqs. (6, S22) are not affected by the distribution of c_i . This is an important result as it reduces the number of relevant parameters necessary to define the temporal evolution of the system.

1.4 Asymptotic theory for networks with distributed β

As we already mentioned, in the *MPN* dataset we find the evolution of social ties described by a distribution of β rather than a single value of it. This observation points to a more heterogeneous distribu-

tion of social attitudes with respect to the other six analyzed datasets. Arguably, such tendency might be driven by the different functions phone calls serve enabling us to communicate with relatives, friends or rather to companies, clients etc.. The need to introduce different values of β in the system complicates the model beyond analytical tractability (see SI for details). Nevertheless, we find that the leading term of the evolving average degree can be described by introducing a simplified model, in which the nodes of the system feature different values of β and undergo a simplified dynamics (see SI for further information) that neglects, for every node, the effects of links established by others. In these settings we can solve the ME and show that the minimum value of β , β_{\min} , rules the leading term of the evolving average degree. In other words, we find that even in this case $\langle k(a, t) \rangle$ evolves as in Eq. (6) but with β substituted by β_{\min} . As shown in Figure S12-D the analytical predictions coming from the simplified model find good agreement with the empirical evidence. It is interesting to notice that the nodes characterized by β_{\min} are those with the weak tendency to reinforce already established social ties. They are social explorers [34]. Notably, our results, indicate that they lead the growth of average connectivity of the network.

2 Discussion

The empirical finding presented here shows clearly that the “cost” associated to the establishment of a new social tie is not constant but is function of the number of already activated ties, thus supporting the idea that social capabilities are limited by cognitive, temporal or other forms of constraints [11, 12, 13]. Framing this empirical finding in a simple stochastic model of network formation, we can derive a general asymptotic theory of the network dynamic and derive the general scaling laws for the behavior in time of the node’s degree and degree distribution.

The model comes with some shortcomings. Indeed, it does not capture the modular structure or, more in general, correlations beyond the nearest neighborhood that are typical of many social networks [35]. In fact, individuals tend to organize their social cir-

cles in tight, often hierarchical, communities. The model does not capture the burstiness typical of social acts [36, 37]. We consider a simplified Poissonian scheme of nodes activation. A recent extension of the activity driven framework, without the reinforcement mechanism acting on social ties, has been proposed to account for non Poissonian node dynamics [38]. This is the natural starting point to generalize our model to bursty activities. Furthermore, the model does not consider the turnover of social ties [34]. Indeed, in our framework once a social connection has been established it cannot be eliminated in favor of others. Clearly, this feature is of particular importance when considering social systems evolving on longer time scales, as the scientific journals we studied here, and might influence the measurement of the parameters describing evolution of the ego-networks.

Notwithstanding these limitations, the modeling framework we propose pave the way to a deeper understanding of the emergence and evolution of social ties. The agreement between the analytical predictions and observed behaviors in seven real datasets, describing different types of social interactions, are encouraging steps in this direction. Finally, our results are a starting point for the development of predictive tools able to forecast the growth and evolution of social systems based not just of regression models or simplified toy models but on a more rigorous analysis of ego-network dynamics.

3 Materials

3.1 Datasets

We analyzed seven large-scale and time resolved networks describing three different types of social interactions.

- Five networks from the APS datasets takes into account the co-authorship networks found in the Journals of the American Physical Society. Specifically, the PRA dataset covers the period from Jan. 1970 to Dec. 2006 and contains 36,880 papers written by 34,093 authors and connected by 100,683 edges. The PRB dataset refers to the Jan. 1970 to Dec. 2007 period and con-

tains 104,047 papers published by 84,367 authors which are connected by 416,048 links. The PRD datasets covers the same period as the PRB one and it is composed by 33,376 papers, 21,202 authors and 60,033 edges. The PRE dataset refers to the Jan. 1993 to Dec. 2006 period with 24,204 papers published by 28,188 authors connected by 68,029 edges. Finally, the PRL dataset contains all the 66,422 papers published between Jan. 1960 to Dec. 2006 and written by 78,763 authors forming 299,017 edges.

- One network dataset describing Twitter mentions (TMN), exchanged by users from January to September 2008. The network has 536,210 nodes performing about 160M events and connected by 2.6M edges.
- One Network dataset describing the mobile phone calls network (MPN) of 6,779,063 users of a single operator with about 20% market share in an undisclosed European country from January to July 2008. The datasets contains all the phone calls to and from company users thus including the calls towards or from 33,160,589 users in the country connected by 92,784,825 edges.

3.2 Asymptotic solution of the ME for distributed β_i values

The solution of Eq. (4) found in Eq. (5) holds if the system feature a single value of β . As already discussed in the MPN dataset we find multiple values of β ranging from a minimum value, β_{\min} to a maximum one β_{\max} . To find a prediction of the long time behavior of such a system, let us propose a simplified model in which we focus on a single agent whose parameters are a_i , β_i and c_i . In this simplified version the agent can only call other nodes in the network, i.e. we neglect the contribution coming from the incoming calls). In this approximation we have to solve a modified version of Eq. (3), obtained by discarding all the terms containing the activity a_j of the nodes $j \neq i$. By repeating the same procedure above, we get to the continuum limit that reads:

$$\frac{\partial P_i(k, t)}{\partial t} = -a_i \left(\frac{c_i}{k}\right)^{\beta_i} \left[\frac{\partial P_i(k, t)}{\partial k} - \frac{1}{2} \frac{\partial^2 P(k, t)}{\partial k^2} \right], \quad (8)$$

whose solution is similar to Eq. (5), the only differences being the value of $\beta = \beta_i$ and the behavior of the $B(a_i, c_i)$ constant (see Materials and Methods and the SI for details). Interestingly, even in this case we find an average degree $\langle k(a, t) \rangle$ growing accordingly to the exponent β_i , i.e. $\langle k(a, t) \rangle \propto (at)^{\frac{1}{1+\beta_i}}$. Now, let us create a reservoir of N distinct nodes of equal activity a and assign to each of them a different value of β_i drawn from an arbitrary distribution $P(\beta_i)$. Let us also group these nodes in B classes, defined so that each class i contains all the nodes featuring a similar value of $\beta \sim \beta_i$. If we now let these N nodes evolve following the simplified model above, the average degree of each class i will grow as $\langle k_i(a, t) \rangle \propto t^{\frac{1}{1+\beta_i}}$. Then, in the long time limit, the minimum value of β_i , i.e. β_{\min} , will lead the growth of the ensemble's average degree (see SI for further details), i.e.

$$\langle k(t) \rangle \propto t^{\frac{1}{1+\beta_{\min}}}. \quad (9)$$

3.3 $F(a)$ and $\rho(k)$ distributions from real data

We implement the method found in [39] to determine the most likely functional form of both the activity and degree distributions. The fitting procedure is as follows: for each functional form of the distribution considered (power law, log-normal, truncated power law and stretched exponential) we first determine the x_{\min} value, i.e. the lower bound to the functional form behavior. The x_{\min} value is defined as the value that minimizes the Kolmogorov-Smirnov (KS) distance between the analytical complementary cumulative distribution (CDF) and the CDF of the data. The latter are found for each value of x_{\min} by computing the optimal parameters of the distribution using the maximum-likelihood estimator (MLE). Then, comparing the CDF($x \geq x_{\min}$) of the data $S(x)$ with the analytical one $P(x)$, we compute the KS-distance as the maximum distance between the two CDF, i.e. $\text{KS}_d(x_{\min}) = \max_{x_i \geq x_{\min}} |S(x_i) - P(x_i)|$. Once all the distances are computed we determine x_{\min} as the values at which the minimum distance is recorded, i.e. $x_{\min} = \min_x \text{KS}_d(x)$ (see SI and [39] for details). Once we compute all the parameters for all

the functional forms analyzed we compare them with the *likelihood ratio test* \mathcal{R} combined with the p -value that gives the statistical significance of \mathcal{R} (see SI for details). The result of this procedure gives us the best candidate for the $F(a)$ for each dataset. We find that a truncated power law is the best candidate for all the APS datasets together with the MPN one. The only exception is the TMN that displays a Log-Normal distribution of activity (see Fig. 1 and SI for details). After we estimate the functional form and the parameters of the activity distribution $F(a)$, Eq. (S22) gives us the possibility to predict both the functional form of the degree distribution $\rho(k)$ and the values of the parameters of such a distribution (e.g. the α exponent in a power-law with cutoff, see Table 3 for details). The degree distribution can then be fitted by optimizing over the non-scale-free parameters for whose values we do not have an analytical or numerical prediction (e.g. the cut-off τ in a power-law with cutoff). Indeed, we are missing the value of the constant in front of the $(at)^{\frac{1}{1+\beta}}$ term in the growth of the average degree $\langle k(a, t) \rangle$ in Eq. (6).

References

- [1] Mark S Granovetter. The strength of weak ties. *American journal of sociology*, pages 1360–1380, 1973.
- [2] Noah Friedkin. A test of structural features of granovetter’s strength of weak ties theory. *Social Networks*, 2(4):411–422, 1980.
- [3] Nan Lin, Walter M Ensel, and John C Vaughn. Social resources and strength of ties: Structural factors in occupational status attainment. *American Sociological Review*, pages 393–405, 1981.
- [4] Mark Granovetter. The strength of weak ties: A network theory revisited. *Sociological Theory*, 1(1):201–233, 1983.
- [5] Jacqueline Brown and Peter Reingen. Social ties and word-of-mouth referral behavior. *Journal of Consumer Research*, 14(3):350–362, 1987.
- [6] Reed E Nelson. The strength of strong ties: Social networks and intergroup conflict in organizations. *Academy of Management Journal*, 32(2):377–401, 1989.
- [7] Daniel Z Levin and Rob Cross. The strength of weak ties you can trust: The mediating role of trust in effective knowledge transfer. *Management Science*, 50(11):1477–1490, 2004.
- [8] Pasquale De Meo, Emilio Ferrara, Giacomo Fiumara, and Alessandro Provetti. On facebook, most ties are weak. *Commun. ACM*, 57(11):78–84, October 2014.
- [9] Julianne Holt-Lunstad, Timothy B Smith, and J Bradley Layton. Social relationships and mortality risk: a meta-analytic review. *PLoS medicine*, 7(7):e1000316, 2010.
- [10] Robin IM Dunbar. The social brain hypothesis. *brain*, 9(10):178–190, 1998.
- [11] Giovanna Miritello, Esteban Moro, Rubén Lara, Rocío Martínez-López, John Belchamber, Sam GB Roberts, and Robin IM Dunbar. Time as a limited resource: Communication strategy in mobile phone networks. *Social Networks*, 35(1):89–95, 2013.
- [12] James Stiller and Robin IM Dunbar. Perspective-taking and memory capacity predict social network size. *Social Networks*, 29(1):93–104, 2007.
- [13] Joanne Powell, Penelope A Lewis, Neil Roberts, Marta García-Fiñana, and RIM Dunbar. Orbital prefrontal cortex volume predicts social network size: an imaging study of individual differences in humans. *Proceedings of the Royal Society B: Biological Sciences*, 279(1736):2157–2162, 2012.
- [14] J.-P. Onnela, J. Saramäki, J. Hyvönen, G. Szabó, D. Lazer, K. Kaski, J. Kertész, and A.-L. Barabási. Structure and tie strengths in mobile communication networks. *Proceedings of the*

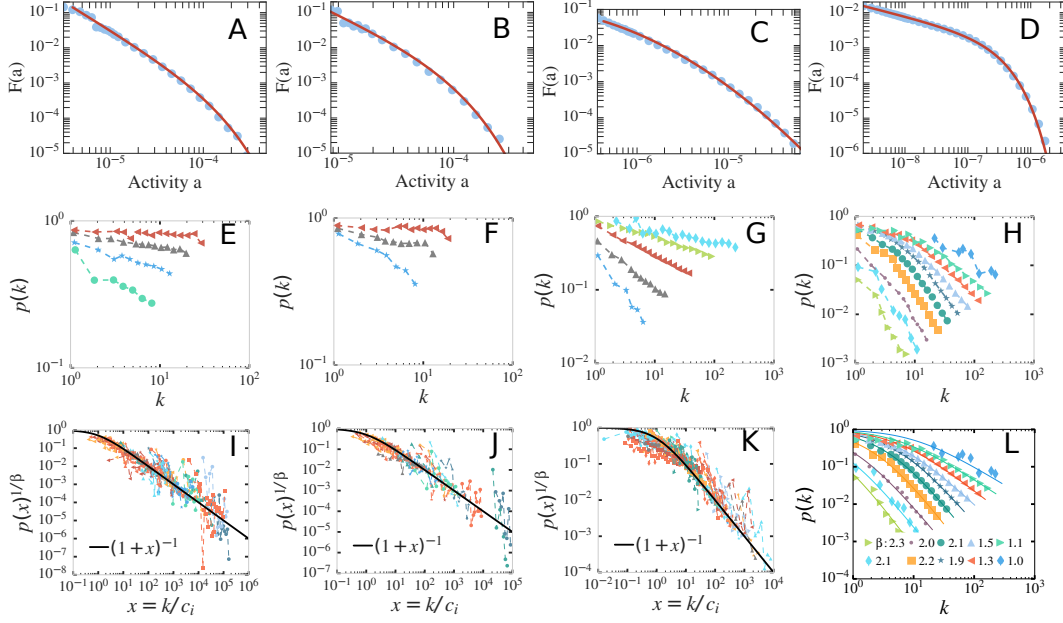


Fig. 1: (A – D) The activity distribution $F(a)$ for PRB (A), PRL (B4, TMN (C) and the MPN (D) dataset. The solid lines represent the fit $F(a)$ with the best functional form for each dataset. The latter are a truncated power law for the PRB, PRL and MPN case, while we find a lognormal for the TWT case (see SI and supplementary materials for details). In these plots we show the experimental data ranging from the lower bound of the fit to the 99.9% of the total amount, thus excluding the higher 0.1% of the measured activity values from the visible area (see materials and SI for details). (E – H) The measured $p_b(k)$ curves for selected nodes classes belonging to the PRB (E), PRL (F), TMN (G) and MPC (H) datasets. Each data sequence (different colors and markers) corresponds to a selected nodes class of the system. As one can see different nodes classes feature a differently behaving attachment rate function $p_b(k)$: for some nodes the probability to attach to a new node quickly drops to 0 at degree $\lesssim 10$ while for some others the attachment probability is still $\gtrsim 0.1$ even at very large degree ($k \sim 10^2$). (I – K) We rescale the attachment rate curves of all the nodes classes of the PRB (I), PRL (J) and TMN (K) datasets by sending $k \rightarrow x_b = k/c_b$ and then plotting the $p_b(x_b)^{1/\beta}$, where β has the same value for every curve. For the MPC dataset (L) we show the original $p_b(k)$ curves belonging to a single nodes class with their fit. The resulting values of β_b are shown in the legend. The latter are found to fall in the $1.0 \lesssim \beta_i \lesssim 2.5$ range.

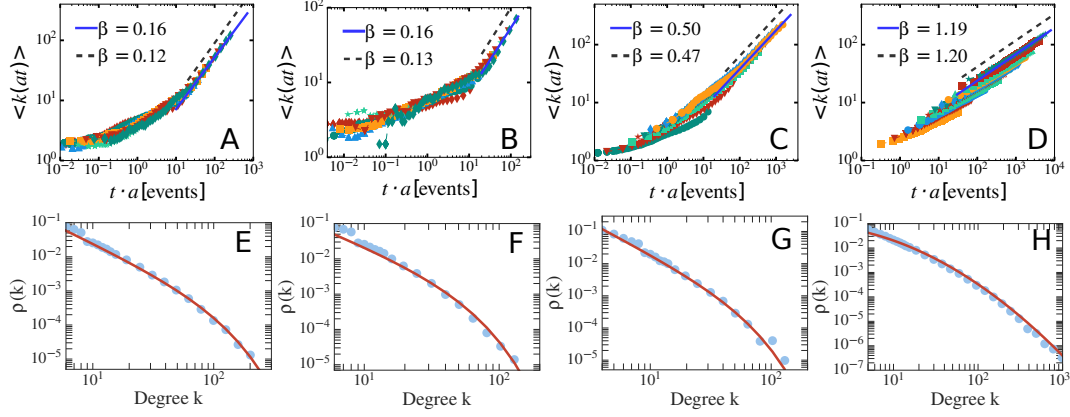


Fig. 2: (A – D) The rescaled $\langle k(at) \rangle$ curves for selected nodes classes belonging to the PRB (A), PRL (B), TWT (C) and MPC (D) datasets. The time of the original data (symbols) is rescaled with the activity value $t \rightarrow at$. We also show the fitting curve $\langle k(t) \rangle \propto t^{\frac{1}{1+\beta}}$ (blue solid lines) and the expected asymptotic behavior (black dashed lines). In the MPC case D we fit using $\beta = \beta_{\min} = 1.2$. (E – H) The degree distribution $\rho(k)$ for the PRB (E), PRL (F), PRA (G) and TMN (H) datasets. The predicted functional form of $\rho(k)$ found in Eq. (S22) and Table (3) is shown for comparison (light blue solid lines). As in Fig. 1 we show the data ranging from the lower bound of the degree distribution to the 99.9% of the data range, thus excluding from the plot area the higher 0.1% of the degree values.

PDF	$F(a)$	$\rho(k)$
Power Law	$a^{-\nu}$	$k^{-[(1+\beta)\nu-\beta]}$
Stret. Exp.	$a^{\nu-1} \exp[-\lambda a^\nu]$	$k^{[(1+\beta)(\nu-1)+\beta]} \exp[-\tau k^{(1+\beta)\nu}]$
Trunc. PL	$a^{-\nu} \exp[-\lambda a]$	$k^{-[(1+\beta)\nu-\beta]} \exp[-\tau k^{(1+\beta)}]$
Log-Normal	$\frac{1}{a} \exp\left[-\frac{(\ln(a)-\mu)^2}{2\sigma_a^2}\right]$	$\frac{1}{k} \exp\left[-\frac{(\ln(k)-\gamma)^2}{2\left(\frac{\sigma_a}{1+\beta}\right)^2}\right]$

Fig. 3: The functional form of the activity PDF $F(a)$ and the predicted functional form of the $\rho(k)$ degree distribution as found in Eq. (S22), i.e. by replacing $a \rightarrow k^{1+\beta}$. This substitution fixes the scale free parameters of the resulting distribution, i.e. the exponent of the power-law and of the k term at the exponent in the first three cases, and the STD $\sigma_k = \frac{\sigma_a}{1+\beta}$ in the Log-Normal case. The free parameters over which we fit the degree distribution are: (i) the cut-off τ in the stretched exponential and power-law with cut-off and (ii) the γ average value in the Log-Normal case. The selected PDF are, from top to bottom: power law, stretched exponential (Stret. Exp.), power law with cutoff (Trunc. PL) and the Log-Normal distribution.

- National Academy of Sciences*, 104(18):7332–7336, 2007.
- [15] M. Karsai, M. Kivelä, R. K. Pan, K. Kaski, J. Kertész, A.-L. Barabási, and J. Saramäki. Small but slow world: How network topology and burstiness slow down spreading. *Phys. Rev. E*, 83:025102, Feb 2011.
 - [16] Márton Karsai, Nicola Perra, and Alessandro Vespignani. Time varying networks and the weakness of strong ties. *Sci. Rep.*, 4:4001, 02 2014.
 - [17] P. Holme and J. Saramäki. Temporal networks. *Physics Reports*, 519:97–125, October 2012.
 - [18] Petter Holme and Jari Saramäki. *Temporal networks*. Springer, 2013.
 - [19] C. Cattuto, W. Van den Broeck, A. Barrat, V. Colizza, J.F. Pinton, and A. Vespignani. Dynamics of person-to-person interactions from distributed rfid sensor networks. *PloS One*, 5(7):e11596, 2010.
 - [20] Lorenzo Isella, Juliette Stehlé, Alain Barrat, Ciro Cattuto, Jean-François Pinton, and Wouter Van den Broeck. What’s in a crowd? analysis of face-to-face behavioral networks. *J. Theor. Biol.*, 271:166, 2011.
 - [21] Juliette Stehlé, Alain Barrat, and Ginestra Bianconi. Dynamical and bursty interactions in social networks. *Phys. Rev. E*, 81:035101, Mar 2010.
 - [22] José Luis Iribarren and Esteban Moro. Impact of human activity patterns on the dynamics of information diffusion. *Physical review letters*, 103(3):038702, 2009.
 - [23] N. Perra, B. Gonçalves, R. Pastor-Satorras, and A. Vespignani. Activity driven modeling of time varying networks. *Sci. Rep.*, 2, 06 2012.
 - [24] Jari Saramäki, E. A. Leicht, Eduardo López, Sam G. B. Roberts, Felix Reed-Tsochas, and Robin I. M. Dunbar. Persistence of social signatures in human communication. *Proceedings of the National Academy of Sciences*, 111(3):942–947, 2014.
 - [25] A. Clauset and N. Eagle. Persistence and periodicity in a dynamic proximity network. In *DIMACS Workshop on Computational Methods for Dynamic Interaction Networks*, pages 1–5, 2007.
 - [26] M. Morris. Telling tails explain the discrepancy in sexual partner reports. *Nature*, 365:437, 1993.
 - [27] Luis EC Rocha, Fredrik Liljeros, and Petter Holme. Information dynamics shape the sexual networks of internet-mediated prostitution. *Proceedings of the National Academy of Sciences*, 107(13):5706, 2010.
 - [28] N. Perra, A. Baronchelli, D. Mocanu, B. Gonçalves, R. Pastor-Satorras, and A. Vespignani. Random Walks and Search in Time-Varying Networks. *Physical Review Letters*, 109(23):238701, December 2012.
 - [29] B Ribeiro, N. Perra, and A. Baronchelli. Quantifying the effect of temporal resolution on time-varying networks. *Scientific Reports*, 3:3006, 2013.
 - [30] R. Pfitzner, I. Scholtes, A. Garas, C.J Tesse, and F. Schweitzer. Betweenness preference: Quantifying correlations in the topological dynamics of temporal networks. *Phys. Rev. Lett.*, 110:19, 2013.
 - [31] Michele Starnini, Andrea Baronchelli, Alain Barrat, and Romualdo Pastor-Satorras. Random walks on temporal networks. *Phys. Rev. E*, 85:056115, May 2012.
 - [32] Eytan Bakshy, Itamar Rosenn, Cameron Marlow, and Lada Adamic. The role of social networks in information diffusion. In *Proc. ACM Intl. World Wide Web Conf. (WWW)*, pages 519–528, 2012.
 - [33] Mario V Tomasello, Nicola Perra, Claudio J Tesse, Márton Karsai, and Frank Schweitzer. The role of endogenous and exogenous mechanisms

- in the formation of r&d networks. *Scientific reports*, 4, 2014.
- [34] Giovanna Miritello, Rubén Lara, Manuel Cebrian, and Esteban Moro. Limited communication capacity unveils strategies for human interaction. *Scientific reports*, 3, 2013.
- [35] Santo Fortunato. Community detection in graphs. *Physics Reports*, 486(3):75–174, 2010.
- [36] Albert-Laszlo Barabasi. The origin of bursts and heavy tails in human dynamics. *Nature*, 435(7039):207–211, 2005.
- [37] Márton Karsai, Kimmo Kaski, Albert-László Barabási, and János Kertész. Universal features of correlated bursty behaviour. *Scientific reports*, 2, 2012.
- [38] Antoine Moinet, Michele Starnini, and Romualdo Pastor-Satorras. Burstiness and aging in social temporal networks. *Physical review letters*, 114(10):108701, 2015.
- [39] Aaron Clauset, Cosma Rohilla Shalizi, and Mark EJ Newman. Power-law distributions in empirical data. *SIAM review*, 51(4):661–703, 2009.
- [40] Jeff Alstott, Ed Bullmore, and Dietmar Plenz. powerlaw: A python package for analysis of heavy-tailed distributions. *PLoS ONE*, 9(1):e85777, 01 2014.
- [41] Michele Starnini and Romualdo Pastor-Satorras. Topological properties of a time-integrated activity-driven network. *Phys. Rev. E*, 87:062807, Jun 2013.

Supplementary Information

S1 Data-sets

S1.1 American Physical Society

The *APS* dataset contains the five co-authorship networks of five journals of the American Physical Society, i.e., *Physical Review A*, *B*, *D*, *E* and Letters (*L*).

The various datasets contains the data referring to all the issues of the single journals from their first issue up to a certain edition, specifically:

- *PRA* from January 1970 to December 2006;
- *PRB* and *PRD* from January 1970 to December 2007;
- *PRE* from January 1993 to December 2006;
- *PRL* from February 1960 to December 2006.

Each dataset is composed by several files (one per month). Each file has as many lines as the number of papers published in that month. Finally, each line contains the IDs of the authors of the specific paper. For instance, the typical head of a file is:

```

Author_000    Author_001    Author_002    #First Paper with 3 authors
Author_003    Author_004
. . .        . . .        . . .        . . .

```

The data are cleaned so as to not take into account the papers with a single author.

When analyzing this dataset we define the user's activity a_i as the number of engaged collaborations (e.g. an author i that publish two papers, the first with 3 co-authors and the second with a single co-author, has activity $a_i = 4$).

S1.2 Twitter Mention Network

The dataset of *Twitter* is composed by 273 daily files covering the period between January the 1st to September the 30th 2008. The dataset contains the so called *fire-hose*, i.e., all the 16,329,466 citations done by all the 536,210 users in the given period. The nodes in the network are connected via 2,620,764 edges.

Each file contains the daily events with the structure:

```

Citer_ID_00    Cited_ID_00    # Event 0
Citer_ID_01    Cited_ID_01    # Event 1
Citer_ID_02    Cited_ID_02    # Event 2
. . .        . . .        . . .

```

This dataset is not cleaned, as we have all the events that happened on the platform in the selected period.

When analyzing this dataset we define the user's activity a_i as the number of citation made by i , i.e. the number of events actually engaged by the node i .

S1.3 Mobile Phone Network

The dataset of the *Mobile Phone Calls (MPC)* is composed by a single file containing the 1,949,624,446 time ordered events with 1 second resolution covering the period between January and July of 2008 for 6,779,063 users of a single operator with 20% market share in an undisclosed European country.

The dataset contains all the events from and toward users of the company (so that even the calls from non-company users to company users and vice-versa are taken into account). As a result, we have 33,160,589 nodes (of which 6,779,063 are users of the selected company) that are connected via 92,784,825 edges.

We split the huge list of events in 98 files (each of them containing more or less the same number of events) for computing convenience. Each file contains events with the structure:

Caller_ID	Called_ID	Company_Caller	Company_Called	# Event 0
Caller_ID	Called_ID	Company_Caller	Company_Called	# Event 1
Caller_ID	Called_ID	Company_Caller	Company_Called	# Event 2
.

where `Company_Caller` and `Company_Called` are the value of the provider company of the called and caller nodes, respectively (e.g. the value is set to 1 if the node is a customer of our company, 0 otherwise).

When analyzing this dataset we define the user's activity a_i as the number of calls done by the node, i.e. the number of calls actually engaged by the node i .

S2 Data analysis

S2.1 Activity distribution and the nodes binning

For the datasets presented in Section S1 we first evaluate, for each node i , the total number u_i of events engaged by the node itself. For instance u_i is the number of calls made by the node i in the *MPC* dataset or the number of citations done by i in the *Twitter* dataset.

We then define the node activity a_i as the ratio between the i -th node's number of events and the total number of events observed in the dataset, i.e. $a_i = u_i/u_{\text{tot}}$ where $u_{\text{tot}} = \sum_j u_j$. Thus, a_i falls in the range $a_i \in [\epsilon, 1.0]$ with $\epsilon = \min_i(u_i)/u_{\text{tot}}$. We then introduce and compute the activity distribution $F(a)$. In Fig. S1 we show the resulting activity distribution for each analyzed dataset, while in Table (1) we show the best candidate functional form for the $F(a)$ distribution of each dataset. The latter is estimated using the methods found in [39].

In particular, we compare the goodness of fit on the $F(a)$ distribution of the functional forms found in Table [1] of the main paper, i.e. power-law, truncated power-law, stretched exponential and log-normal distribution. The procedure for each dataset and each functional form reads as follows:

- we fit the $F(a)$ taking into account all the nodes featuring $a_i \geq x_{\min}$, where x_{\min} is the lower bound of the distribution. The fit is performed using the maximum likelihood estimators (MLE) that return the optimal values of the parameters;
- once the optimal parameters are found we compute the Kolmogorov-Smirnov distance ($KD_d(x_{\min})$) between the analytical and experimental complementary cumulative distribution function (CDF);
- we then apply this procedure for different x_{\min} and set the $a_{\min} = \min_{x_{\min}} KS_d(x_{\min})$ lower bound value as the one that minimizes the KS_d .

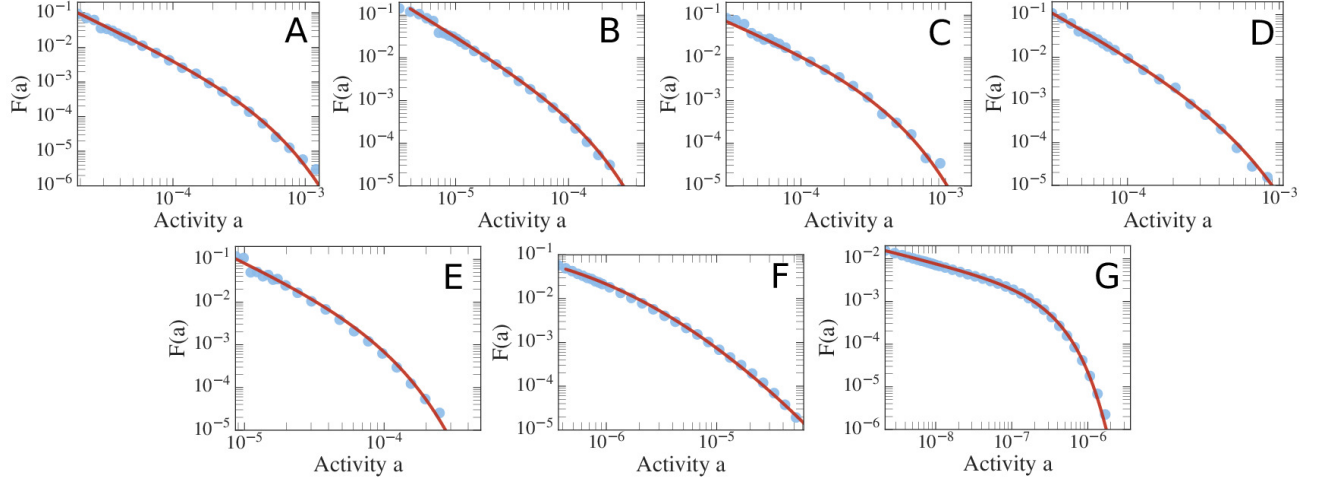


Fig. S1: The experimental activity distribution $F(a)$ for (A) PRA, (B) PRB, (C) PRD, (D) PRE, (E) PRL, (F) TMN and (G) MPN (blue points). We also show the best candidate fit of the $F(a)$ distribution (blue solid lines) featuring the functional form and parameters found in Table (1). In all the plots we show the data and fit ranging from the lower bound x_{\min} to the 99.9% of the measured data, thus excluding from the visible area the top 0.1% of the activity values (see Table (1) for the lower bound details).

Dataset	Distribution	Parameters	KS_d	%	\mathcal{L}
TMN	Lognormal	$a_{\min} = 4.28e - 7, \mu = -14.02, \sigma = 1.71$	$1.5e - 2$	52	$-2.26e + 3$
PRA	Truncated	$a_{\min} = 1.90e - 5, \lambda = 3.14e + 3, \alpha = 1.789$	$1.5e - 2$	32	-301
PRB	Truncated	$a_{\min} = 6.31e - 6, \lambda = 7.96e + 3, \alpha = 1.638$	$1.4e - 2$	41	-744
PRD	Truncated	$a_{\min} = 4.54e - 5, \lambda = 4.02e + 3, \alpha = 1.37$	$1.6e - 2$	27	-286
PRE	Truncated	$a_{\min} = 4.24e - 5, \lambda = 3.32e + 3, \alpha = 1.92$	$1.5e - 2$	23	-264
PRL	Truncated	$a_{\min} = 1.10e - 5, \lambda = 1.55e + 4, \alpha = 1.47$	$1.7e - 2$	31	-577
MPN	Truncated	$a_{\min} = 2.17e - 9, \lambda = 3.82e + 6, \alpha = 0.448$	$9.5e - 3$	94	$-1.6e + 4$

Tab. 1: The candidate functional form of the activity distribution for each analyzed dataset, the evaluated parameters (see Table [1] in the main for the analytical expressions), the Kolmogorov-Smirnov distance KS_d , the percent % of nodes in the dataset that have activity $a_i \geq a_{\min}$ and the normalized log-likelihood \mathcal{L} . In the parameters we include a_{\min} that is the value of the activity that minimizes the KS distance. This is the lower bound for the functional form behavior, i.e. the point at which data behave as the functional form.

We then repeat this procedure for all the functional forms of the $F(a)$ and we then compare them with the *likelihood ratio test* \mathcal{R} combined with the p -value that gives the statistical significance of \mathcal{R} [39, 40]. The result of this procedure gives us the best candidate for the $F(a)$ for each dataset as shown in Table (1). We find that a truncated power law is the best candidate for all the APS datasets together with the MPN one. On the other hand, in the TMN we find a log-normal distribution as the best candidate for the dataset.

Our datasets provide evidence that nodes within the same activity class (i.e. node with similar values of activity a_i) can feature very different memory behavior. In particular agents with large activity may connect to very few different nodes (strong reinforcement) or establish new links at almost every step (weak reinforcement). For this reasons each node i of the network is naturally classified according to her activity a_i and her final degree k_i , i.e. the total number of different agents that have been connected to i in the considered time window.

We then define a binning procedure that let us group together the similar nodes, i.e. nodes with similar activity and final degree. We divide the nodes in N_{act} activity classes so that within each activity class the most active node performs at most 1.5 times the events of the least active node. Then, with the same procedure, we further group the nodes within each activity class a according to their final degree, thus defining $N_{\text{deg}}(a)$ final degree classes. The nodes are therefore divided in $N_b = \sum_{a=1}^{N_{\text{act}}} N_{\text{deg}}(a)$ activity-degree classes. From now on, unless differently stated, whenever we mention the nodes' class or bin b we will be referring to one of these N_b classes.

S2.2 The reinforcement process

To measure the reinforcement process of each system, we count all the communication events $e_b(k)$ engaged by every node i of the b -th class when it has degree $k_i = k$. In other words, $e_b(k)$ is the total number of events engaged by the nodes of the b -th class at degree k .

Each time an event engaged by a node i of the b -th class results in a degree increase $k_i = k \rightarrow k_i = k + 1$, we increment the counter $n_b(k)$ by 1. In other words, $n_b(k)$ is the total number of events that the nodes belonging to the b -th and featuring degree k perform toward a new node. Of course, if a node i of the b -th class with degree $k_i = k$ increases its degree to $k_i = k + 1$ because it gets called by a new node, the $n_b(k)$ counter is not incremented.

The best estimate of the probability for a new node to get establish a new connection at degree k then reads:

$$f_b(k) = \frac{n_b(k)}{e_b(k)}, \quad (\text{S1})$$

where $n_b(k)$ and $e_b(k)$ are the event counters as defined above. We can give an estimate of the uncertainty on $f_b(k)$, by assuming that at a given degree k the events are independent (i.e. there are no correlations between users) and by checking that $1 \ll n_b(k) \ll e_b(k)$ so that the STD $\sigma(f_b(k))$ of $f_b(k)$ reads:

$$\sigma(f_b(k)) = \sigma_b(k) = \sqrt{\frac{f_b(k)(1 - f_b(k))}{e_b(k)}}. \quad (\text{S2})$$

We then fit $f_b(k)$ with the proposed reinforcement function $p_b(k, \beta)$:

$$p_b(k, \beta) = \left(1 + \frac{k}{c(b)}\right)^{-\beta}, \quad (\text{S3})$$

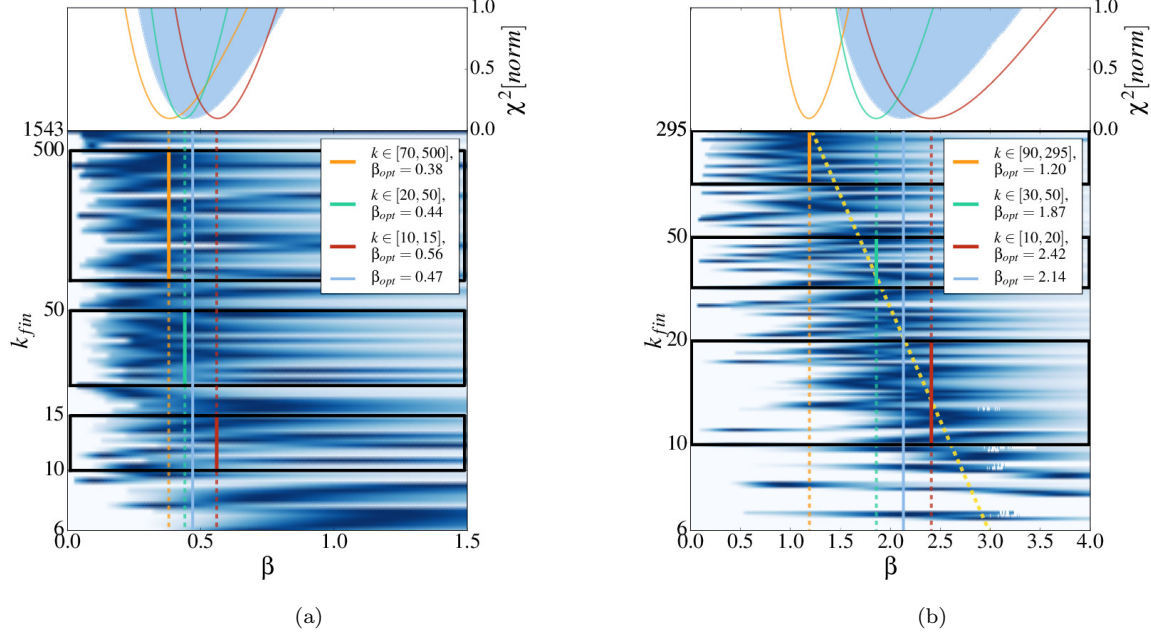


Fig. S2: The heat-map-like value of $-\ln[\chi_b^2(\beta)]$ (bottom plots). We plot the exponent β on the x -axes and the different bins b sorted by their final degree on the y -axes. The color-map is proportional to $-\ln[\chi_b^2(\beta)]$ representing the goodness of fit: the darker, the higher. The cyan vertical line is the value of β_{opt} defined in Eq. (S6), while the other vertical lines represent the same quantity evaluated in the three black boxes corresponding to different final degree intervals. (Top plots) The curve $\chi^2(\beta)$ as defined in Eq. (S5) (up-filled curve) and the same quantity for the three final degree intervals. For Twitter (a): a single value of $\beta_{opt} = 0.47$ fits most of the curves and only some bins b deviate from the average behavior. (b) MPC: in this case we observe different behaviors depending on the final degree. Thus, a single $\beta_{opt} = 2.14$ does not fit all the curves. We also show a “guide-to-the-eye” to highlight this feature (yellow dashed line).

where $c(b)$ is the social propensity of the b -th bin, k is the cumulative degree and β is the reinforcement strength, that will be kept fixed for all the nodes in the system. In particular, for each class b and with a fixed β , we optimize the parameter $c(b)$, by minimizing the function $\chi_b^2(\beta)$:

$$\chi_b^2(\beta) = \sum_{k=1}^{K_b} \frac{[f_b(k) - p_b(k, \beta)]^2}{\sigma_b(k)^2}, \quad (\text{S4})$$

where the index k runs over the K_b points of the b -th bin's curve and $\sigma_b(k)$ is as defined in Eq. (S2). By repeating this procedure for each value of $\beta \in [0, 5.0]$ we find, for each class b , a $\chi_b^2(\beta)$ curve.

In Fig. S2 we show the behavior of $\chi_b^2(\beta)$. For each class b we find a minimum of $\chi_b^2(\beta)$ at a certain $\beta_{opt}(b)$ (see the horizontal lines in the heat-map-like panels of Fig. S2).

Moreover, Fig. S2 shows that there are two different behaviors. Specifically, in the TMN case (see Fig. S2 (a)), one value of $\beta_{opt} = 0.47$ fits most of the curves, exception made for some outsiders: the value of $\beta_{opt}(b)$ that maximizes the $1/\chi_b^2(\beta)$ is practically the same for all the bins. On the contrary, in the MPC case the

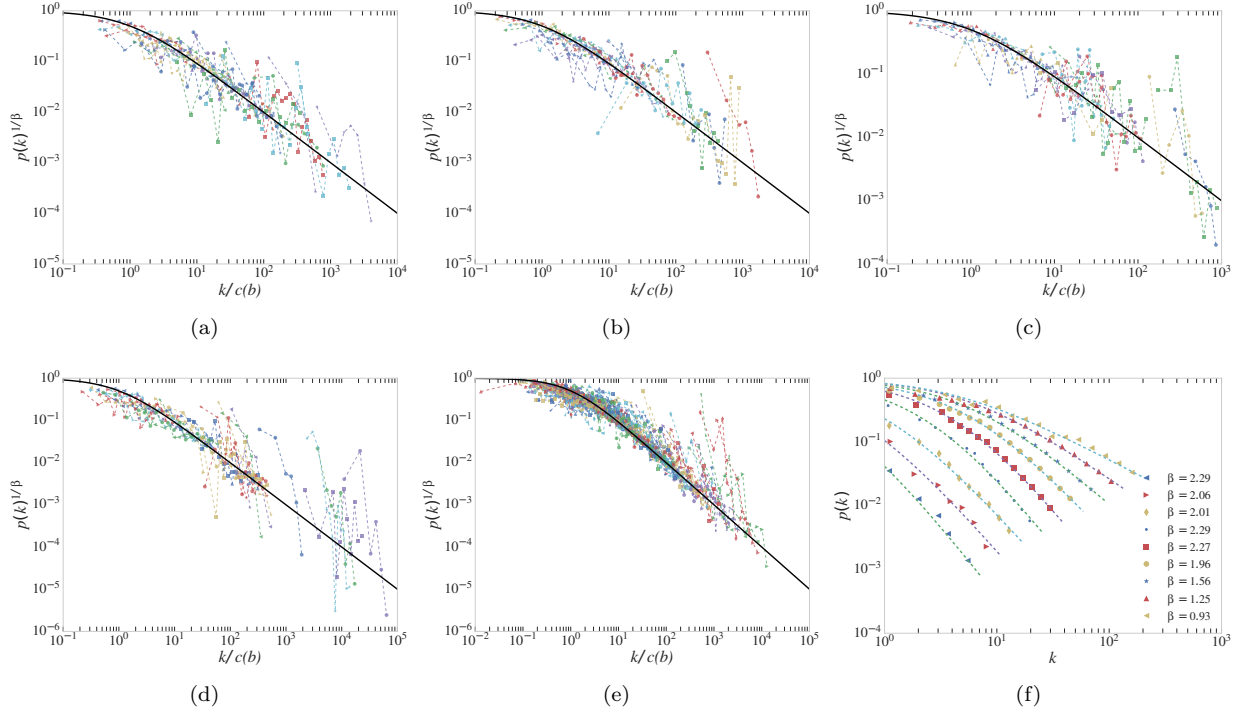


Fig. S3: Plot of the experimental $p_b(k)$ curves for the (a) PRA, (b) PRD, (c) PRE, (d) PRL, (e) TMN and (f) MPC datasets. In the (a-e) cases the k is rescaled as $k \rightarrow k/c(b)$, where $c(b)$ is the constant for the b -th class curve at $\beta = \beta_{\text{opt}}$. The $p_b(k/c(b))$ points are then rescaled sending $p_b(k/c(b))^{1/\beta_{\text{opt}}}$. In the (f) panel for MPC we simply plot $p_b(k)$ as a function of k with no rescaling, given that each curve features its own β optimal value β_{opt} as shown in the legend.

maximum of the $1/\chi_b^2(\beta)$ function follows a diagonal path ranging from a larger $\beta_{\text{opt}}(b)$ for bins with lower final degree to a smaller $\beta_{\text{opt}}(b)$ for larger degree bins. In this case a single β_{opt} cannot fit all the curves and we have to consider a multi- β model where each class b features a different optimal value of β , $\beta_{\text{opt}}(b)$.

In Fig. S3 we present the rescaled $p_b(k)$ curves for the PRA, PRD, PRE, PRL, TMN and MPC datasets. In the first five cases we show the rescaled curves obtained by substituting $k \rightarrow k/c_b$ and then plotting $p_b(k) \rightarrow p_b(k)^{1/\beta_{\text{opt}}}$. As one can see, the curves nicely collapse on the reference curve $(1+k)^{-1}$. In the MPC case we show instead the original curves, each one fitted with its own $\beta_{\text{opt}}(b)$. The latter parameter falls in the $1.2 \lesssim \beta_{\text{opt}}(b) \lesssim 3.0$ interval for most of the curves as we also show in Fig. S2.

To quantitatively define the β_{opt} parameter, let us define the total mean square deviation $\chi^2(\beta)$ as

$$\chi^2(\beta) = \sum_{b=1}^{N_b} [\chi_b^2(\beta)], \quad (\text{S5})$$

where N_b is the total number of curves, i.e. the number of activity-degree bins b . Then, for the single exponent case, the function $\chi^2(\beta)$ allows to define β_{opt} as:

$$\beta_{\text{opt}} = \min_{\beta} (\chi^2(\beta)). \quad (\text{S6})$$

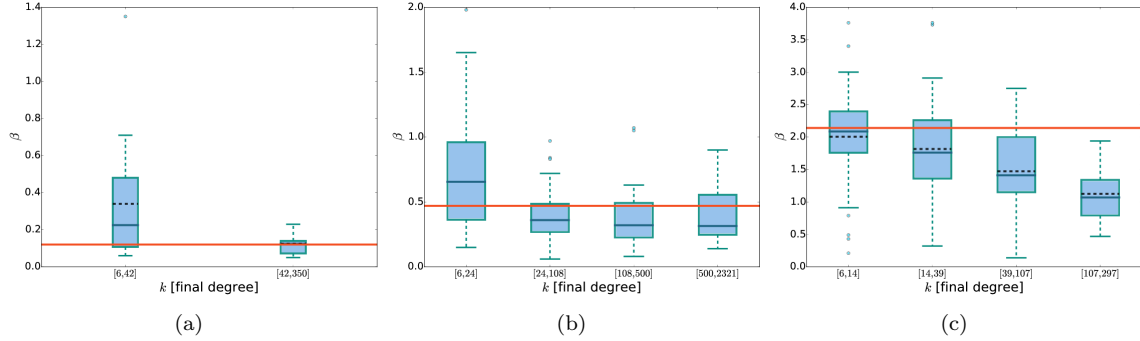


Fig. S4: The box plot representing the distribution for different range of nodes classes b of the $\beta_{\text{opt}}(b)$ for (a) PRB, (b) TMN and (c) MPN. We also show the global optimal value β_{opt} (horizontal red line) as found in Eq. (S6). The height of the box corresponds to the lower and upper quartile values of the distribution and the horizontal solid line corresponds to the distributions median, while the dashed lines indicates the average value for each range of final degree. The whiskers extend from the box to values that are within $1.5x$ the quartile range. As one can see, in both the PRB and TMN datasets the optimal values β_{opt} is compatible with the distribution found in all the nodes class ranges (we find the same result for all the other APS datasets analyzed). On the other hand, in the MPN the distribution of $\beta_{\text{opt}}(b)$ lowers as the final degree of the class increases. The last group of nodes classes is no more compatible with the overall optimal β_{opt} , being the distribution centered around $\beta_{\text{opt}} \sim 1.1$, in agreement with our estimation of $\beta_{\text{min}} = 1.2$.

In the multi- β case instead, we compute the different values of the exponent $\beta_{\text{opt}}(b)$ found in the system by grouping the memory classes b accordingly to their final degree as shown in Fig. S2. The optimal value of $\beta_{\text{opt}}(b)$ is found to be minimum for the bins featuring a large final degree, i.e. $\beta_{\text{min}} \equiv \beta_{\text{opt}} \sim 1.2$, which, as we will show in Section S3.2.3, is the exponent driving the evolution of the network.

To corroborate the results just outlined, we show in Fig. S4 the box plot of the $\beta_{\text{opt}}(b)$ distribution for different groups of nodes classes b grouped by their final degree. We note that the APS and TWT datasets are well approximated by a single β_{opt} as the distribution of $\beta_{\text{opt}}(b)$ within each sub-group of nodes is compatible with the global optimal value β_{opt} . On the other hand, in the MPN case we see that the large final-degree classes have their $\beta_{\text{opt}}(b)$ distribution centered around a smaller value of $\beta_{\text{min}} \sim 1.2$. As already anticipated, this value will lead the asymptotic growth of the system as we will show in Section S3.2.3.

As a last remark we present in Fig. S5 (a, b) the measured distribution of the constant $c(b)$ for the MPN and TMN datasets. We show the distribution for all the nodes in the network and for each activity class a , i.e. the group of nodes featuring similar activity. The values of these constants are distributed but peaked around an average value. Moreover, the distribution of the $c(b)$ parameter within each activity closely follows the global one. The distribution of the social attitude $c(b)$ then appears to be a global, activity independent feature of the nodes in the system. Finally, in Fig. S5 (c) we show how the average value of the $c(b)$ constants, $\langle c \rangle = \langle c(b) \rangle_b$, differs from one dataset to the other varying from $\langle c \rangle = 0.8$ in PRB to $\langle c \rangle = 1.7$ in TMN and $\langle c \rangle = 4.6$ in the MPN case, respectively.

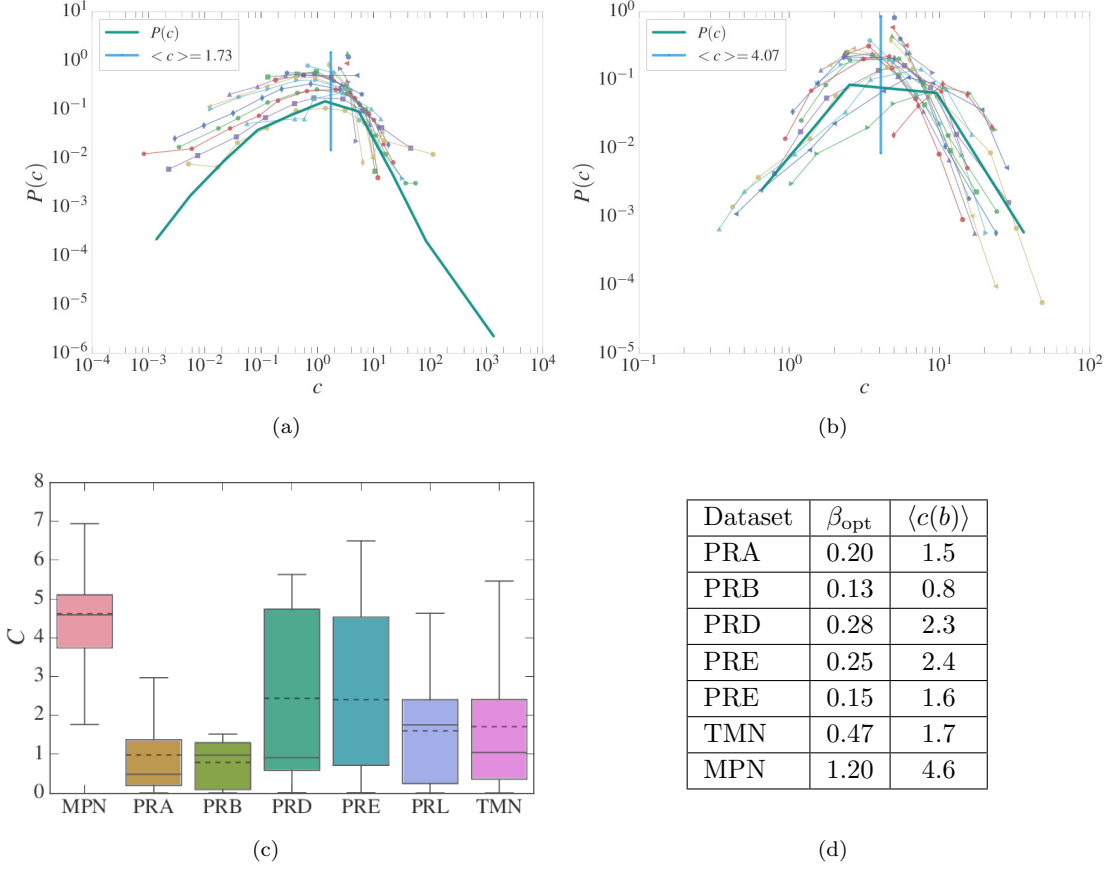


Fig. S5: The $P(c)$ distribution of the constant $c(b)$ for the (a) TMN, and (b) MPN case (solid green line). We also compare the global $P(c)$ distribution with the distribution of the $c(b)$ values found within each activity class (solid lines and points): we find that the distribution of the $c(b)$ parameter is more or less activity independent as most of the distribution of the single activity classes follows the same functional form of the total distribution $P(c)$. We then report the average value $\langle c \rangle$ of the $c(b)$ constant for each dataset (vertical cyan line). The latter reads 1.71 for TMN and 4.62 for MPN. Note that in the single β case we evaluate $c(b)$ as the values of $c(b)$ that best fits the b -th $p_b(k, \beta)$ curve fixing β at its optimal value ($\beta = \beta_{\text{opt}}$). On the other hand, in the multi- β case we evaluate $c(b)$ as the ones that best fits the $p_b(k, \beta(b))$ curve, where the exponent is now foxed to the $\beta(b)$ value for the memory class b , i.e. to the optimal value for the class b . (c) The box plot showing the global distribution of the constant $c(b)$ in all the datasets analyzed. The height of the box corresponds to the lower and upper quartile values of the distribution and the horizontal solid line corresponds to the distributions median, while the dashed lines indicates the average value for each range of final degree. The whiskers extend from the box to values that are within $1.5x$ the quartile range. (d) In this table we report all the values of the reinforcement exponent β_{opt} and the average reinforcement constant $\langle c(b) \rangle$. For the MPN case we report the $\beta_{\text{opt}} = \beta_{\text{min}}$ and the constant values are evaluated for each nodes class b using its optimal value of β , $\beta_{\text{opt}}(b)$.

S3 The model

S3.1 Activity driven networks with no memory

The activity driven networks are an effective framework to describe time varying networks. The simplest memory-less model is defined as follows: the network consists of N nodes featuring an activity potential a_i , i.e. the probability for a node i to get active in a certain time interval dt reads $a_i dt$. The evolution rules are: (i) at each time step we start with N disconnected nodes; (ii) each node i whether gets active with probability $a_i dt$ or does not activate with probability $(1 - a_i) dt$. If a node gets active it calls a randomly selected node j in the network, thus creating an edge e_{ij} . (iii) At the end of the time step all the created connection are deleted and we start again from the initial step (i).

These evolution rules define the Master Equation (ME) for $P_i(k, t)$, i.e. the probability that a node i of activity a_i has degree k at time t , where the degree k is the number of nodes that contacted i up to time t . We also set, without losing generality, $dt = 1$. The discrete time equation for $P_i(k, t)$ then reads:

$$P_i(k, t + 1) = \quad (S7)$$

$$\begin{aligned} & a_i \frac{N - k}{N} P_i(k - 1, t) + a_i \frac{k}{N} P_i(k, t) + P_i(k - 1, t) \sum_{j \sim i} a_j \sum_h \frac{P_j(h, t)}{N} + \\ & P_i(k, t) \sum_{j \sim i} a_j \sum_h P_j(h, t) \frac{N - 1}{N} + P_i(k, t) \sum_{j \sim i} a_j + P_i(k, t) (1 - \sum_j a_j). \end{aligned} \quad (S8)$$

The equation is obtained in the approximation where $a_i \ll 1$, so that between two consecutive times $t_i = t$ and $t_{i+1} = t + 1$ only one site can be active. We will assume that the activity a_i of a node i is small, i.e. $0 < a_i \ll 1$, and we will also consider the approximation $1 \ll k \ll N$ i.e. the integrated number of neighbors of a site is much larger than 1 but much smaller than the total number of agents N . The first term of the sum represents the probability that the site i is active and a new link is added to the system. The second term is the probability that the site i is active but this site connects to a site that has been already linked. In the third and fourth terms, the symbol $\sum_{j \sim i}$ denotes the sum over the sites that are not yet connected to i . In particular, the third term represents the probability that one of these sites is active and that it connects to i . The fourth term is the probability that one of these sites is active but no link between j and i is established. The fifth term is the probability that one of the sites already connected to i is active (being $\sum_{j \sim i}$ the sum over the nodes already connected to i); in this case no new link is added to i . Finally, the last term represents the probability that at time t all the sites are not active. For $k \ll N$, the second term can be neglected. After some algebra we obtain the equation:

$$P_i(k, t + 1) - P_i(k, t) = - (P_i(k, t) - P_i(k - 1, t)) \left(a_i + \frac{1}{N} \sum_{j \sim i} a_j \right)$$

given that $\sum_h P_j(h, t) = 1$. For $k \ll N$, we assume that $\frac{1}{N} \sum_{j \sim i} a_j = \langle a \rangle$ i.e. the average value of the activity. In the limit of large time and large k we can write a continuous equation in t and k obtaining:

$$\frac{\partial P_i(k, t)}{\partial t} = (a_i + \langle a \rangle) \left(-\frac{\partial P_i(k, t)}{\partial k} + \frac{\partial^2 P_i(k, t)}{\partial k^2} \right). \quad (S9)$$

The solution of Eq. (S9) is straightforward:

$$P_i(k, t) = (2\pi(a_i + \langle a \rangle)t)^{-\frac{1}{2}} \exp\left(-\frac{(k - (a_i + \langle a \rangle)t)^2}{2t(a_i + \langle a \rangle)}\right). \quad (\text{S10})$$

In the large time limit this solution reduces to a delta function: $P(a, k, t) = \delta(k - (a + \langle a \rangle)t)$ Therefore, the average degree $\langle k(a, t) \rangle$ of the nodes of activity a grows as:

$$\langle k(a, t) \rangle \propto (a + \langle a \rangle)t. \quad (\text{S11})$$

as already found in [23, 41]. Moreover the asymptotic degree distribution $\rho(k)$ of a network with activity distribution $F(a) \propto a^{-\nu}$ is:

$$\rho(k) \propto k^{-\nu}. \quad (\text{S12})$$

S3.2 Plugging in the reinforcement process

The model presented in Sec. S3.1 is a basic model as it contains no correlations on an agent's story at all. In particular, the probability for a node i to re-call an already contacted node is independent of the node degree. While simple to describe and solve analytically, this model is not realistic, as there are no correlations in the each agent's history. Moreover, the probability to call an already contacted node is always small as $k/N \ll 1$ (and thus the probability to call a new node remains ~ 1 even at large degree k). However, as shown in Sec. S2.2, real-world systems features a strong reinforcement process, as the probability $p_i(k)$ to call a new node at degree k decreases as the degree k increases.

For this reason we introduce an extended version of the model described in [16] et al. which includes a reinforcement function $p_i(k)$ that measures the probability for an active node i , that has already contacted k different nodes in the network, to call a new node instead of an already contacted one.

S3.2.1 The single β case

As already shown in Sec. S2.2 the functional form for the reinforcement process $p_i(k)$, i.e. the probability of adding a new link for the node i of degree k , reads:

$$p_i(k) = (1 + k/c_i)^{-\beta}. \quad (\text{S13})$$

By plugging Eq. (S13) into Eq. (S8) for node i , we get:

$$\begin{aligned} P_i(k, t+1) = & P_i(k-1, t) \left[a_i p_i(k-1) + \sum_{j \not\sim i} a_j \sum_h \frac{p_j(h)}{(N-h)} P_j(h, t) \right] + \\ & P_i(k, t) \left[a_i [1 - p_i(k)] + \sum_{j \not\sim i} a_j \sum_h \left(1 - \frac{p_j(h)}{N-h} P_j(h, t) \right) \right] + \\ & P_i(k, t) \left[1 - \sum_j a_j \right], \end{aligned} \quad (\text{S14})$$

where N is the number of nodes in the network, $\sum_{j \not\sim i}$ is the sum over the nodes not yet connected to i and \sum_j is the sum over all the N nodes of the network. Each term of Eq. (S14) corresponds to a particular

event that may take place in the system, as already presented in the paper. For instance, the first term of the l.h.s. of Eq. (S14) takes into account the increment of the node i 's degree from $k - 1$ to k . This may happen whether because node i gets active and contacts a new node in the system with probability $a_i p_i(k - 1)$ or because a node j never contacted before gets active and calls exactly node i with probability $a_j p_j(h)/(N - h)$, being h the degree of j . In the same way, the second line takes into account that node i does not change degree k whether because it calls an already contacted node or because the non contacted nodes call other nodes in the network. The last line of Eq. (S14) considers the possibility that no node in the network gets active.

If we now substitute Eq. (S13) in Eq. (S14), after some algebra we get:

$$\begin{aligned} P_i(k, t + 1) - P_i(k, t) = & \frac{a_i c_i^\beta}{(k - 1 + c_i)^\beta} P_i(k - 1, t) - \frac{a_i c_i^\beta}{(k + c_i)^\beta} P_i(k, t) \\ & - (P_i(k, t) - P_i(k - 1, t)) \sum_{j \sim i} a_j \sum_h \frac{P_j(h, t) c_j^\beta}{(N - h)(h + c_j)^\beta}. \end{aligned} \quad (\text{S15})$$

Then, by applying the same approximations of large degree k and time t we obtain the continuous equation:

$$\begin{aligned} \frac{\partial P_i(k, t)}{\partial t} = & -a \frac{c_i^\beta}{k^\beta} \frac{\partial P_i(k, t)}{\partial k} + \frac{a_i c_i^\beta}{2k^\beta} \frac{\partial^2 P_i(k, t)}{\partial k^2} + \frac{a_i \beta c_i^\beta}{k^{\beta+1}} P_i(k, t) + \\ & \left(\frac{1}{2} \frac{\partial^2 P_i(k, t)}{\partial k^2} - \frac{\partial P_i(k, t)}{\partial k} \right) \int da_j F(a_j) a_j \int dc_j \rho(c_j | a_j) \int dh \frac{c_j^\beta}{h^\beta} P_j(h, t), \end{aligned} \quad (\text{S16})$$

where $\rho(c_j | a_j)$ is the probability for a node j of activity a_j to have reinforcement constant c_j .

The long time asymptotic solution of Eq. (S16) is of the form:

$$P_i(k, t) \propto \exp \left[-A \frac{(k - C(a_i, c_i) t^{\frac{1}{1+\beta}})^2}{t^{1/(1+\beta)}} \right], \quad (\text{S17})$$

Moreover, $C(a, c)$ is a constant depending on the activity a and the reinforcement constant c that follows the:

$$\frac{C(a, c)}{1 + \beta} = \frac{ac^\beta}{C(a, c)^\beta} + \int da' F(a') \int dc' \rho(c' | a') \frac{a' c'^\beta}{C(a', c')^\beta}. \quad (\text{S18})$$

We do not have an exact solution for $C(a, c)$, however $C(a, c) \simeq (ac^\beta)^{1/(1+\beta)}$ for large a .

Let us note that Eq. (S17) can be obtained setting the variable $x = k - C(a) t^{\frac{1}{1+\beta}}$ and substituting it in Eq. (S16) and imposing that $|x| \ll t^{\frac{1}{1+\beta}}$ from Eq. (S16):

$$\begin{aligned} \frac{\partial P_i(x, t)}{\partial t} = & \frac{a_i \beta c_i^\beta}{C(a_i, c_i)^{1+\beta} t} \left(x \frac{\partial P_i(x, t)}{\partial x} + P_i(x, t) \right) + \frac{C(a_i, c_i)}{2(1 + \beta) t^{\frac{\beta}{1+\beta}}} \frac{\partial^2 P_i(x, t)}{\partial x^2} \\ & - \frac{\partial P_i(x, t)}{\partial x} \int da_j F(a_j) \int dc_j \rho(c_j | a_j) \int dy \frac{a_j \beta c_j^\beta}{C(a_j, c_j)^{1+\beta} t} P_j(y, t) y. \end{aligned} \quad (\text{S19})$$

The solution of the latter equation is of the form

$$P_i(x, t) \approx t^{-\frac{1}{2(1+\beta)}} \exp \left(-\frac{Ax^2}{t^{1/(1+\beta)}} \right) \quad (\text{S20})$$

thus confirming that x can be considered much smaller than $t^{\frac{1}{1+\beta}}$.

An important consequence of equations (S17) and (S18) is that, for a system featuring a reinforcement strength β , the average degree of the nodes belonging to a class b of activity a and constant c grows as:

$$\langle k(a, c, t) \rangle \propto C(a, c) \cdot t^{\frac{1}{1+\beta}}. \quad (\text{S21})$$

In particular, $\langle k(a, c, t) \rangle \propto (at)^{\frac{1}{1+\beta}}$ for large values of the activity a .

As expected, the average degree grows slower than in the memoryless case ($\beta = 0$) where the average degree grows linearly in time, as found in Eq. (S11). Moreover, the presence of a reinforcement process also affects the asymptotic behavior of $\rho(k)$. Indeed, as already shown in the main paper, Eq. (S21) gives us the relation between the degree k and the activity a at a given time t , as $k \propto a^{\frac{1}{1+\beta}}$. Thus, given an activity distribution $F(a)$, we can infer the functional form of the degree distribution $\rho(k)$ by substituting $a \rightarrow k^{\frac{1}{1+\beta}}$, finding:

$$\rho(k)dk \propto F(k^{(1+\beta)})k^\beta dk. \quad (\text{S22})$$

Specifically, by supposing a power-law activity distribution $F(a) \propto a^{-\nu}$ and considering that the degree distribution for a class b is described by Eq. (S17), we obtain

$$\rho(k) \propto k^{-[(1+\beta)\nu-\beta]}. \quad (\text{S23})$$

where we integrated over time t and reinforcement constant $c(b)$ and we considered the asymptotic regime of large time and activity.

S3.2.2 Numerical results

We performed numerical simulations to check the result of Section S3.2.1. We fix the following parameters:

- $N = 10^6$ nodes;
- activity $a \in [\epsilon, 1.0]$ with $\epsilon = 10^{-3}$, power-law distributed so that $F(a) \propto a^{-\nu}$ with $\nu = 2.1$;
- single value of the reinforcement exponent $\beta = \{0.5, 1.0, 1.5, 2.0\}$ and a fixed $c = 1$ for all the nodes;
- $T = 10^5$ evolution steps.

We start with no edge in the system and we draw for each node the activity a_i from the distribution $F(a)$. At each step a randomly chosen node gets active with probability a_i . An active node then connects with probability $p_i(k)$ with a randomly chosen node which have not been yet connected to i or, with probability $1 - p_i(k)$, the node calls an already contacted node and no new connection is added to the system. An evolution step corresponds to N of these elementary steps, i.e. for each evolution step we give, on average, the possibility to make a call to every node in the network.

The results are in excellent agreement with the analytical predictions. First, in Fig. S6 we show that the analysis presented in Section S2.1 correctly recovers the reinforcement exponent β_{opt} . Indeed the minimum of the $\chi_b^2(\beta)$ are vertically aligned with the value of β fixed in the simulations.

Then, in Fig. S7 we present the asymptotic growth of the average degree for an activity class (i.e. a collection of nodes bins b featuring similar activity values) and we compare it with the analytical prediction

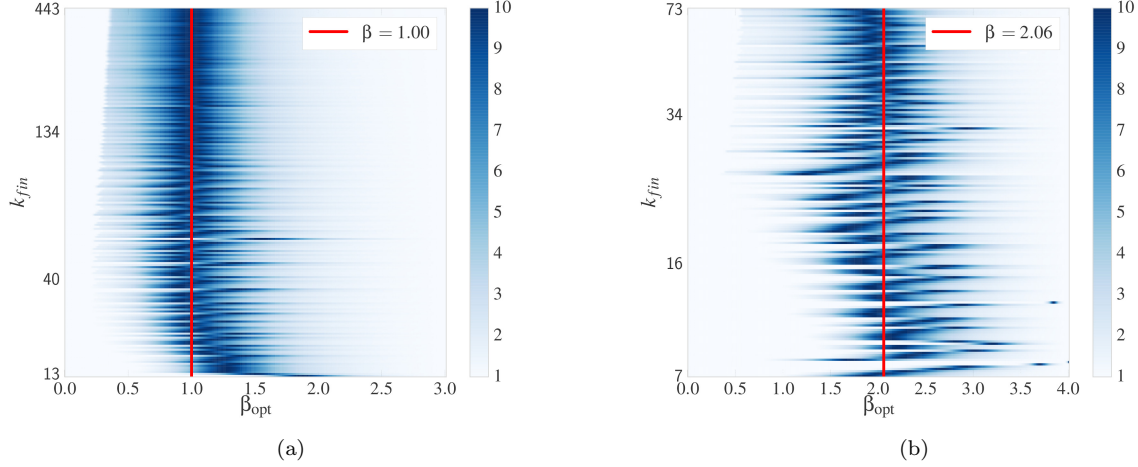


Fig. S6: The heat-map of $-\ln(\chi_b^2(\beta))$ obtained from the simulation in the same way as in Figure S2 from real data. As one can see the recovered β_{opt} is in excellent agreement with the value used in the simulation: 1.0 in the (a) panel and 2.06 in the (b) panel.

$\langle k(a, t) \rangle \propto (at)^{\frac{1}{1+\beta}}$. In Fig. S8 we show that the shape and the evolution of the $P_i(k, t)$ distribution follows the predicted form of Eq. (S17).

The last check regards the overall degree distribution $\rho(k)$ that should follow Eq. (S23). In Fig. S9 we compare the activity distribution $F(a) \propto a^{-\nu}$ and the degree distribution $\rho(k)$. The exponent μ leading the $\rho(k) \propto k^{-\mu}$ is in good agreement with the analytically predicted value $\mu = [(1 + \beta)\nu - \beta]$.

S3.2.3 The multi- β case

As shown in Section S2 a single value of the reinforcement exponent β is found to fit most of the $p_b(k)$ curves in both the *APS* and *TMN* datasets, while for *MPN* a single value of β cannot fit all the $p_b(k)$ curves for each activity-degree class b at once. For this reason we further develop the model, letting each node i to feature three parameters: the activity a_i and the reinforcement constant c_i together with the exponent β_i of the underlying reinforcement process.

Since the model with three parameters per node is difficult to handle, we apply some approximations in order to get analytical insight. In particular, we work in simplified single-agent framework, where we focus on a single agent that can only connect to other nodes and never get called. Within this approximation the master equation for the node i reads:

$$P_i(k, t + 1) = a_i p(k - 1) P_i(k - 1, t) + P_i(k, t) [a_i(1 - p(k)) + (1 - a_i)]. \quad (\text{S24})$$

The continuum limit for large degree k and time t of Eq. (S24) is:

$$\frac{\partial P}{\partial t} = -a \left(\frac{c}{k}\right)^\beta \left[\frac{\partial P}{\partial k} - \frac{1}{2} \frac{\partial^2 P}{\partial k^2} \right]. \quad (\text{S25})$$

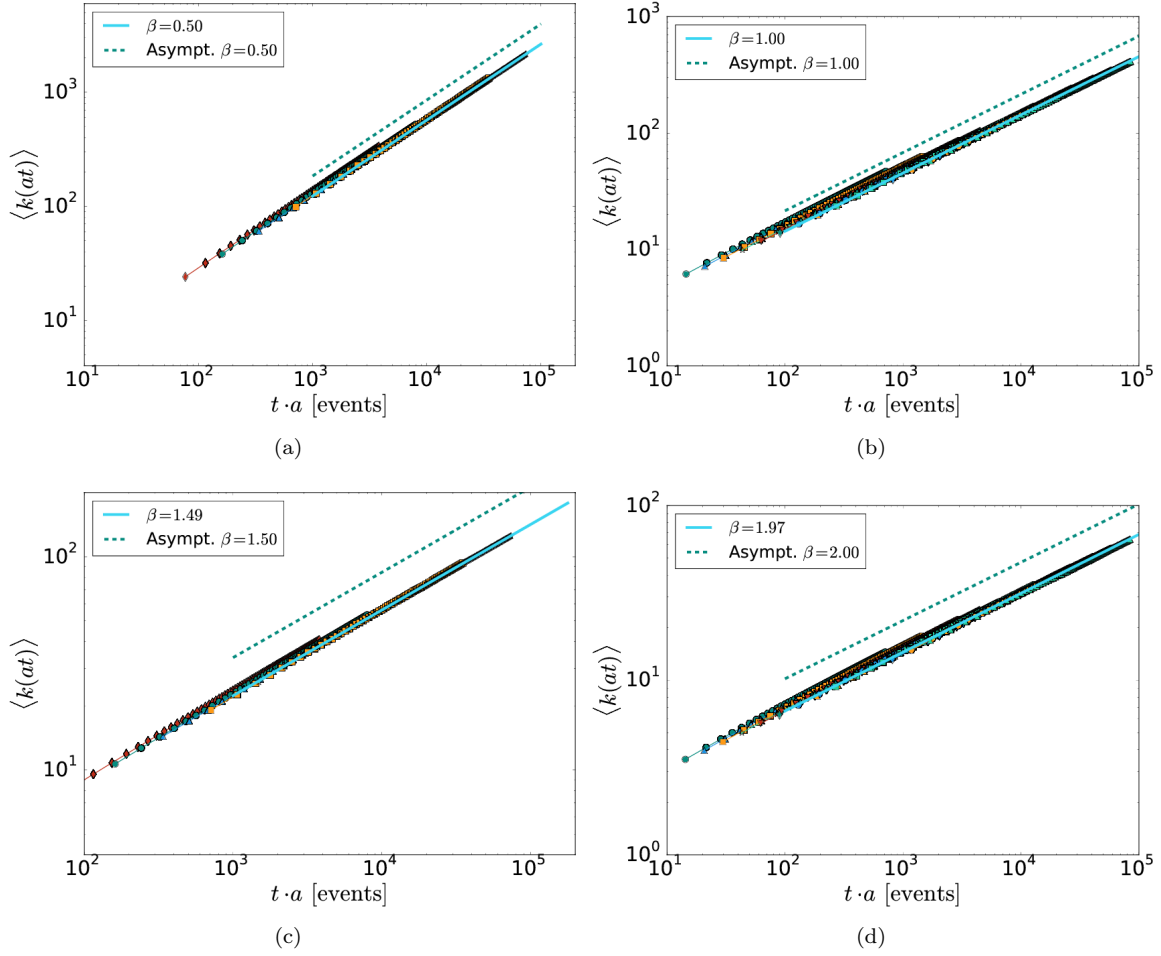


Fig. S7: The average degree $\langle k(at) \rangle$ for different activity classes in the $\beta = 0.5$ (a), $\beta = 1.0$ (b), $\beta = 1.5$ (c) and $\beta = 2.0$ (d) case. The time is rescaled with activity $t \rightarrow at$, so that all the curves collapse on a single behavior. We also fit $\langle k(at) \rangle \propto (t/A)^{\frac{1}{1+\beta}}$ (cyan solid line) and compare the simulation with the analytical result $\langle k(at) \rangle = A \cdot t^{\frac{1}{1+\beta}}$ (blue dashed line).

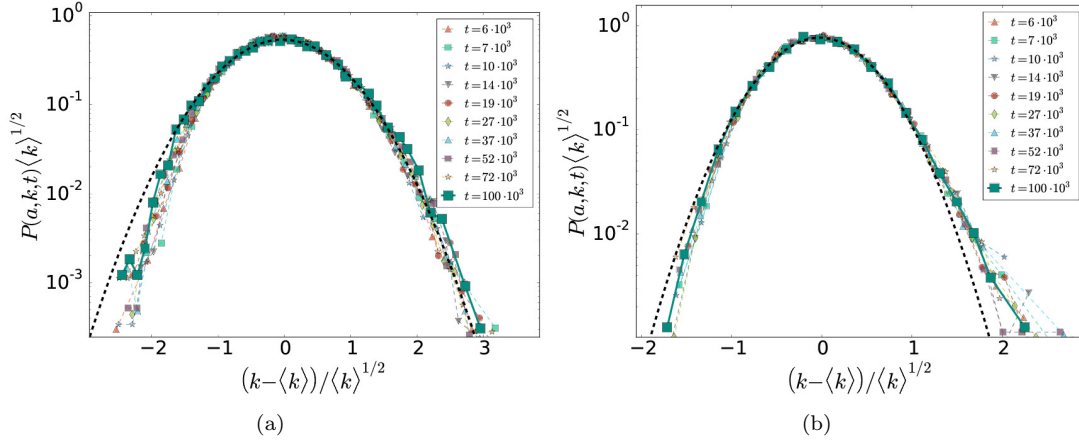


Fig. S8: The probability distribution $P_a(k, t)$ for a selected activity class a in the simulations with exponent $\beta = 1.0$ (a) and $\beta = 2.0$ (b). We compare different evolution times (see legend) by rescaling the degree $k \rightarrow \tilde{k} = (k - \langle k(a, t) \rangle) / \langle k(a, t) \rangle^{1/2}$ on the x -axis and the distribution itself $P_a(k, t) \rightarrow \langle k(a, t) \rangle^{1/2} P(a, \tilde{k}, t)$ on the y -axis, where $\langle k(a, t) \rangle$ is the average degree at time t for the nodes belonging to the activity class a . We also show the fit of the large time $P(a, k, t)$ with a Gaussian curve (black dashed line) as predicted in Eq. (S17).

The solution for $P_i(k, t)$ is:

$$P_i(k, t) \propto \exp \left[-A \frac{\left(k - C_i t^{\frac{1}{1+\beta_i}} \right)^2}{t^{1/(1+\beta_i)}} \right], \quad (\text{S26})$$

where the C_i now reads:

$$C_i = [(1 + \beta_i) c_i^\beta a_i]^{\frac{1}{1+\beta_i}}. \quad (\text{S27})$$

Again, the average degree $\langle k_i(t) \rangle$ grows as:

$$\langle k_i(t) \rangle \propto C_i t^{\frac{1}{1+\beta_i}}. \quad (\text{S28})$$

The result found in Eq. (S28) holds for a single class of nodes with a given set of activity a_i and reinforcement constant c_i and strength β_i .

The average degree $\langle k(a, t) \rangle$ for the activity class a can be computed by integrating over the different values of β_i and c_i :

$$\langle k(a, t) \rangle = \int dc' \int d\beta' \rho(\beta', c' | a) C(a, c', \beta')(t)^{\frac{1}{1+\beta'}} \quad (\text{S29})$$

where $\rho(\beta, c | a)$ is the probability for a node of activity a to have a reinforcement exponent and constant equal to β and c . By assuming that the distribution of the exponent β is independent from a and c we can factor out the time-depend term obtaining for the activity class a :

$$\langle k(a, t) \rangle \propto \int d\beta' \rho(\beta') t^{\frac{1}{1+\beta'}}, \quad (\text{S30})$$

where $\rho(\beta)$ is the probability distribution of the β parameter.

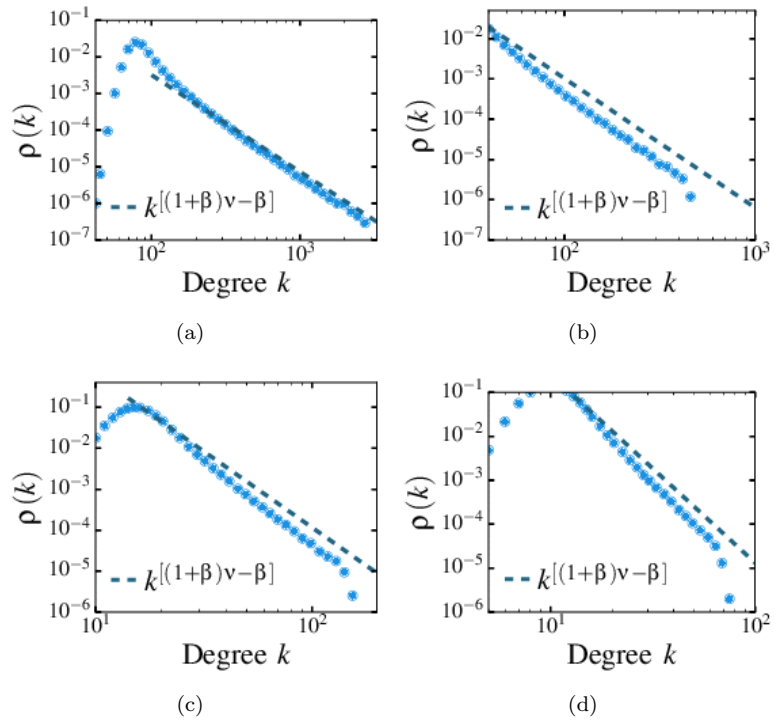


Fig. S9: The resulting degree distribution of simulations featuring $\beta = 0.5$ (a), $\beta = 1.0$ (b), $\beta = 1.5$ (c) and $\beta = 1.0$ (d). The analytical predictions (given $F(a) \propto a^{-\nu}$, with $\nu = 2.1$) for the scaling exponent are shown (blue dashed lines).

Let us assume that $\rho(\beta)$ can be written as a sum of Kroenecker δ -functions, i.e.:

$$\rho(\beta) = \frac{1}{\sum_i C_i} \sum_{i=1}^{N_\beta} C_i \delta(\beta - \beta_i). \quad (\text{S31})$$

By plugging Eq. (S31) in Eq. (S30) we find that:

$$\langle k(a, t) \rangle \propto \sum_{i=1}^{N_\beta} C_i t^{\frac{1}{1+\beta_i}} \xrightarrow{t \rightarrow \infty} t^{\frac{1}{1+\beta_{\min}}}, \quad (\text{S32})$$

so that the minimum value of β_i , β_{\min} leads the asymptotic behavior of the $\langle k(a, t) \rangle$ function.

S3.2.4 Numerical results

To investigate the multi- β case we performed further numerical simulations considering networks with the following parameters:

- $N = 10^6$ nodes;
- activity $a \in [\epsilon, 1.0]$ with $\epsilon = 10^{-3}$, power -law distributed so that $F(a) \propto a^{-\nu}$ with $\nu = 2.1$;
- (a) reinforcement exponent $\beta = [0.5, 1.5, 2.5]$ with probability $[1/6, 1/3, 1/2]$ (i.e. one sixth of the nodes has $\beta = 0.5$, one third $\beta = 1.5$ and a half of them $\beta = 2.5$ regardless of their activity) and (b) $\beta = [1.0, 1.5, 2.0]$ with equal probability $1/3$.
- fixed $c = 1$ for all the nodes;
- $T = 2 \cdot 10^5$ evolution steps.

The numerical procedure is similar to the one described in Section S3.2.2, the difference being that we compute the attachment probability $p_i(k)$ taking into account the reinforcement exponent β_i of the node itself.

In Fig. S10 we show that, in both the cases, we can recover the behavior described in Section S2.1 for real data. In particular Fig. S10(a) (related to the $\beta \in [1, 2]$ case) we observe a clear diagonal pattern of the optimal values of the exponent $\beta(b)$ for the b bins that minimize the $\chi_b^2(\beta)$. In particular $\beta(b)$ varies from $\beta \sim 2.0$ values for lower degree nodes bins up to $\beta \sim 1.0$ values for the larger final degree nodes bins. The figure recalls the situation of the MPC dataset presented in Fig. S2 (b) and in the main paper.

In Fig. S11 we show the asymptotic growth of the average degree $\langle k(a, t) \rangle$ together with the predicted asymptotic behavior proportional to $t^{\frac{1}{1+\beta_{\min}}}$. As one can see, numerical results and the suggested analytical solution are in very good agreement in both the cases.

S3.3 Comparison with real data

In Fig. S12 we present the comparison between prediction and real data for the PRA, PRB, PRD, PRE, TMN and MPN datasets. The $\langle k(a, t) \rangle$ curve of each activity class is shown with the time rescaled with the activity of each activity class, i.e. $t \rightarrow at$. In the MPC case we use as $\beta_{\text{opt}} = \beta_{\min} = 1.2$ (the β value found in the largest degree bins of Fig. S2 (b)). In all the other cases, as the β_{opt} fits correctly most of the curves, we use the β_{opt} value returned by our analysis.

Finally, in Fig. S13 we present the degree distributions, together with the predicted functional form of degree distribution as found in Table (1) in the main paper.

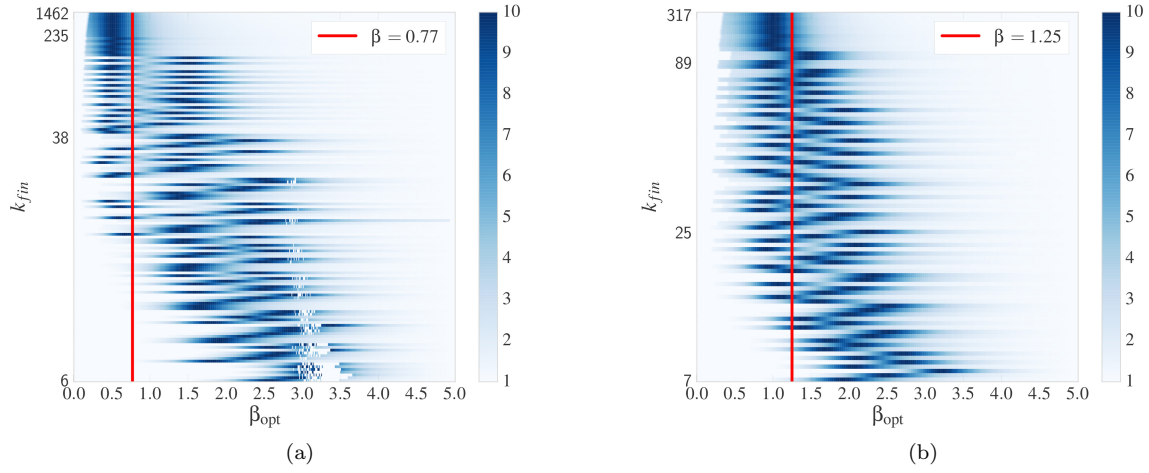


Fig. S10: The heat-map like matrix of $-\ln(\chi^2(\beta))$ for the simulation with $\beta \in [0.5, 1.5, 2.5]$ (a) and $\beta \in [1.0, 1.5, 2.0]$ (b); analogous to Figure S2 for real data.

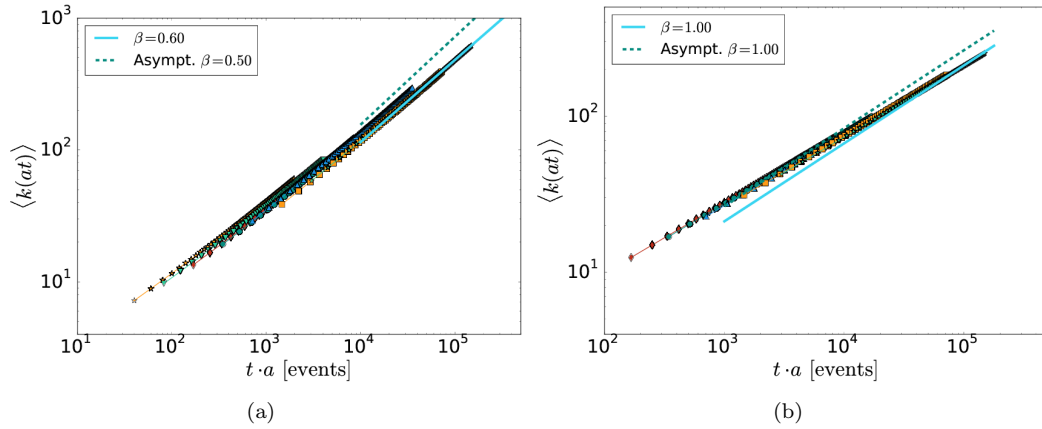


Fig. S11: The average degree $\langle k(at) \rangle$ for different activity classes in the (a) $\beta \in [0.5, 1.5, 2.5]$ and (b) $\beta \in [1.0, 1.5, 2.0]$ case. The time is rescaled with activity $t \rightarrow at$, so that all the curves collapse. We also plot the fit $\langle k(at) \rangle \propto (t/A)^{\frac{1}{1+\beta^*}}$ in the long time limit (cyan solid line) and the predicted asymptotic growth $\langle k(at) \rangle = A \cdot t^{\frac{1}{1+\beta_{\text{min}}}}$ (dashed line).

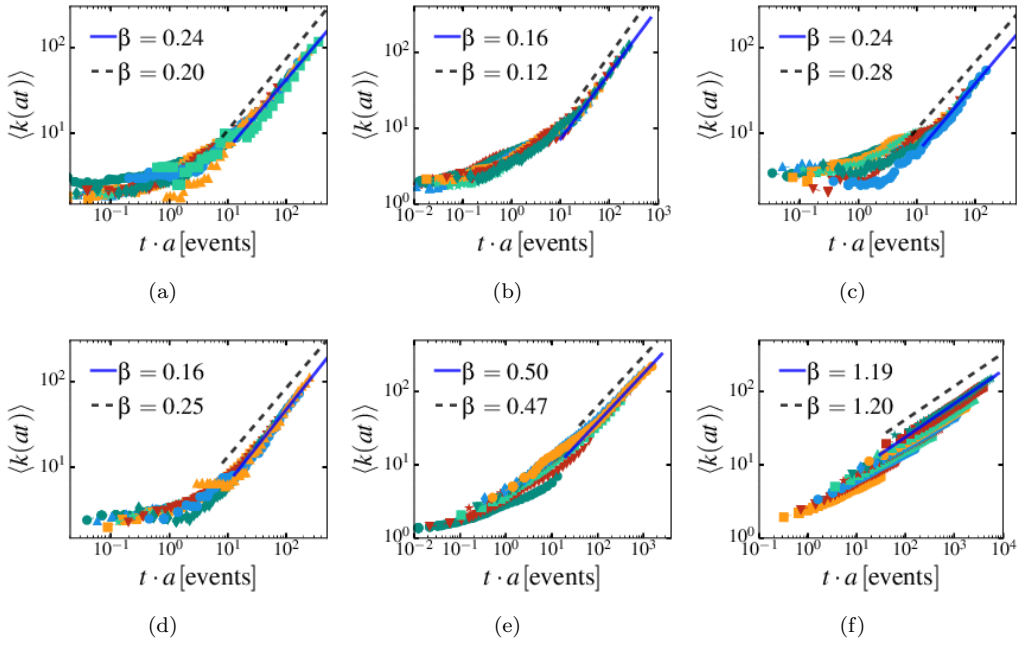


Fig. S12: The average degree $\langle k(at) \rangle$ (each data series corresponds to a different activity class) for: (a) PRA, (b) PRB, (c) PRD, (d) PRE, (e) TWT and (f) MPC. We compare the data for $\langle k(a, t) \rangle$ with the expected behavior (dashed lines) $(at)^{1/(1+\beta_{\text{opt}})}$: in panels (a-e) β_{opt} has been evaluated according Eq. (S6), while in the (f) case we use $\beta_{\text{opt}} = \beta_{\text{min}} = 1.2$. We also plot the power-law fit $\langle k(a, t) \rangle \propto (at)^{1/(1+\beta^*)}$ (solid lines) for comparison.

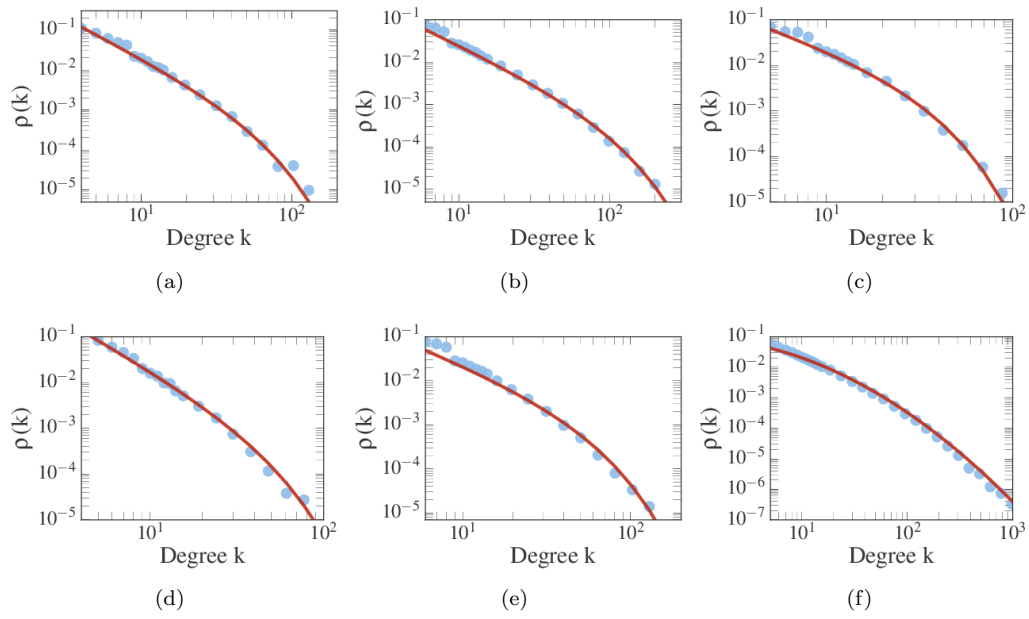


Fig. S13: The degree distribution $\rho(k)$ for: (a) PRA, (b) PRB, (c) PRD, (d) PRE, (e) PRL and (f) TMN (blue circles). We compare the results with the predicted behavior of Table (1) of main paper given the parameters of Table (1) (red solid lines). We use the single value of β_{opt} defined by Eq. (S6) in all the cases. As in Fig. S1 we show the data and fit ranging from the lower bound to the 99.9% of the measured data, thus excluding from the visible area the top 0.1% of the degrees values.